

# A surface renewal model to analyze infrared image sequences of the ocean surface for the study of air-sea heat and gas exchange

C. S. Garbe

Interdisciplinary Center for Scientific Computing, University of Heidelberg, Heidelberg, Germany

U. Schimpf

Institute of Environmental Physics, University of Heidelberg, Heidelberg, Germany

B. Jähne

Interdisciplinary Center for Scientific Computing, University of Heidelberg, Heidelberg, Germany

Received 30 January 2003; revised 18 February 2004; accepted 15 July 2004; published 27 August 2004.

[1] Thermographic techniques are presented that directly measure the temperature difference across the thermal boundary layer at the sea surface, the probability density function of surface renewal, the net heat flux, and the heat transfer velocity during nighttime. The techniques are based on a model of surface renewal. Through the use of digital image processing techniques, temporally and spatially highly resolved measurements are feasible, limited only by the thermal imager. We present laboratory measurements from the Heidelberg Aeolotron and field measurements from the GasExII cruise taken at a spatial resolution of 3 mm and temporal resolution of 10 ms. The net heat flux estimates of the thermographic techniques and micrometeorological methods agree with an error less than 5% for conditions in which the surface renewal model is applicable. Experimental evidence is presented for the probability density function of surface renewal to be best described by a logarithmic normal distribution. At moderate and high wind speeds when the influence of surface films is not significant, surface renewal seems to be an adequate model for air-water heat exchange. *INDEX TERMS:* 4504 Oceanography: Physical: Air/sea interactions (0312); 4572 Oceanography: Physical: Upper ocean processes; 4568 Oceanography: Physical: Turbulence, diffusion, and mixing processes; *KEYWORDS:* surface renewal, air-sea heat transfer, net heat flux

**Citation:** Garbe, C. S., U. Schimpf, and B. Jähne (2004), A surface renewal model to analyze infrared image sequences of the ocean surface for the study of air-sea heat and gas exchange, *J. Geophys. Res.*, 109, C08S15, doi:10.1029/2003JC001802.

## 1. Introduction

[2] Current state of the art techniques for measuring the transfer velocities of gases are based on mass balance methods where tracer concentrations in the water are artificially modified and changes are measured over time. The effect of changes in concentration caused by diffusion due to currents in the ocean can be accounted for by introducing a second tracer with a different diffusivity, a technique known as the dual tracer method [Geernaert, 1999; Fairall *et al.*, 2000]. These methods yield point measurements with integration times as long as days. Recently direct eddy correlation techniques have been introduced [McGillis *et al.*, 2001]. Here the integration times are shortened somewhat to make measurements on timescales of less than an hour feasible. Still these measurements present point measurements with integration times too long to predict and link the transfer velocities to small-scale interactions, often taking place on

timescales of less than seconds. The same problems hold true for measurements of the transport of heat. While the different techniques may help in relating the mean transfer velocities to other mean quantities such as wind speed, roughness of the sea surface or whitecap coverage and thus help in finding semiempirical parameterizations, they are not adequate for gaining a deeper understanding of the transport processes involved.

[3] The use of an infrared camera with its spatially resolved temperature measurement opens up new possibilities for studying air-water heat transfer. Spatial structures of the upper most ten micrometers are observable, which allows one to draw conclusions about the transport processes involved [Haußecker, 1996] and an analysis of the predominant scales of turbulence [Schimpf, 2000]. The use of infrared cameras for measurements at the sea surface have found wider acceptance, as other parameters important to transport processes such as Langmuir circulations [Veron and Melville, 2001], wave-breaking dynamics [Jessup *et al.*, 1997a] and microscale wave breaking [Jessup *et al.*, 1997b] can be detected with such devices as well. Still, the unsolved

issue of estimating heat fluxes directly at the air-water interface at high temporal and spatial resolution prevails. Only by measuring the heat flux and the small-scale processes influencing the transfer of heat on the same spatial and temporal scales simultaneously, can a deeper understanding of the transport phenomena involved be attained.

[4] A temperature difference  $\Delta T$  or concentration difference  $\Delta C$  will lead to the transport of heat or mass, expressed by the heat flux  $j_h$  or mass flux  $j_g$ . Because of the linearity of both Fourier's and Fick's laws for the transport of heat and mass respectively, this transport can be expressed by the transfer velocity  $k$  independent of the concentration difference. For the transport of heat, this velocity is defined by

$$k_{\text{heat}} = \frac{j}{\rho c_p \Delta T}, \quad (1)$$

with the density  $\rho$  and the specific heat  $c_p$  of seawater.

[5] The technique described in this paper relies heavily on the similarity in between the transport of heat and that of masses, such as gas tracers. Strong experimental evidence exists, backing up this assumption [Jähne *et al.*, 1989, 1998]. Only through this similarity in transport can results gained for the transport of heat be applied to the transport of mass. The relation of the heat transfer velocity  $k_h$  and the mass transfer velocity of a certain gas  $k_g$  is given by

$$\frac{k_g}{k_h} = \left( \frac{Sc_h}{Sc_g} \right)^n, \quad (2)$$

where  $Sc_h$  and  $Sc_g$  are the Schmidt numbers of heat and gas respectively and  $n$  the Schmidt number exponent [Jähne *et al.*, 1998]. From this equation the gas transfer velocity  $k_g$  can be deduced from the heat transfer velocity  $k_h$  since the Schmidt numbers are known.

[6] This paper is organized as follows: In section 2 the underlying model of surface renewal is introduced. On the basis of this model a technique for estimating the temperature difference across the thermal boundary layer  $\Delta T$  is outlined in section 3. Apart from  $\Delta T$ , its temporal change in a Lagrangian frame of reference is needed for estimating the parameters of air-sea heat transfer. In section 4 it is shown how to compute the material derivative of  $\Delta T$  from infrared images employing digital sequence analysis. From the knowledge of  $\Delta T$  and its material derivative the residence time of water parcels in the thermal layer  $\tau$ , the net air-water heat flux  $j$  and the transfer velocity of heat  $k_h$  can be computed. It is shown in section 5 how to compute  $\tau$ , in Section 6 how to deduce the pdf of surface renewal from this estimate of  $\tau$ , in section 6 two methods for estimating  $j$  and in section 7 the estimation of  $k_h$ . Assumptions and limitations of the presented techniques are addressed in section 8. Finally, the experimental setup is outlined in section 9 followed by laboratory measurements in section 10 and in situ measurements in Section 11.

## 2. Surface Renewal Model

[7] When studying transport phenomena at the sea surface it is important to have an understanding of the basic physical processes involved. Generally the turbulent structures underneath the interface are very complex and difficult to understand fully, both experimentally and theoretically. Simplified model assumptions are vital to gain insight into the predominant processes which in turn allows for indi-

rectly measuring important quantities of air-sea mass and heat exchange. Except in high wind speed regimes, where a substantial part of the transfer of soluble gases is due to bubbles [Asher and Wanninkhof, 1993], the fundamental structures of transport of both mass and heat are similar. Under this limitation the model presented in the following is the same for both entities transported. Since bubble mediated gas transfer is not considered by the model, discrepancies between model prediction and actual measurements can thus be attributed to this mode of transport, presenting an indirect measurement thereof.

[8] Considerable success has been obtained with a simple model which allows small parcels of water adjacent to the interface to be replaced randomly by water from the well mixed turbulent layers from the bulk of the water. This so-called surface renewal model has been introduced in chemical engineering by Higbie [1935], who assumed periodic renewal of the water parcels. The model was then extended in chemical engineering to include statistically distributed random events by Danckwerts [1951], Hariott [1962], and Rao *et al.* [1971]. It was later applied to the air-sea interface by Brutsaert [1975b], Brutsaert [1975a], Liu and Businger [1975], Liu *et al.* [1979], Jähne [1980], and [Soloviev and Schlüssel [1994].

[9] In this model the motion of the molecular sublayer can be expected to remain locally laminar and parallel to the interface. As such the seawater at the sea surface cannot be easily replaced by the water from the bulk, although it can come very close to it. It is instructive to consider an individual fluid parcel in the mixing layer. Because of the very high efficiency of turbulent transport it will be at the same temperature  $T_{\text{bulk}}$  of the bulk. Because of a stochastic renewal process it will be moved very close to the interface. The sea surface is subject to the net heat flux  $j$ , composed of the sensible heat flux  $j_{\text{sens}}$  due to conduction, the latent heat flux  $j_{\text{lat}}$  due to evaporative cooling, and the long-wave radiative heat flux  $j_{\text{rad}}$ . During daytime, short-wave fluxes due to solar irradiation will also be present. These are of no concern here as only measurements during nighttime are under consideration. As opposed to short-wave solar irradiation, which is a volumetric source of heat, the fluxes present during the night are only effective directly at the sea surface. Once injected into the boundary layer by the renewal process, the water parcels equilibrate with the surface. This equilibration takes places by thermal conduction as formulated in Fourier's law. This process is of course very similar to that of mass transport, where Fick's laws of diffusion are applicable. Assuming that horizontal gradients are negligible in comparison to vertical gradients and further employing a constant flux boundary condition at the interface, the following expression for the sea surface temperature  $T_{\text{surf}}$  can be derived [Soloviev and Schlüssel, 1996]:

$$T_{\text{surf}}(t) = \alpha j \sqrt{t - t_0} + T_{\text{bulk}}, \quad t \geq t_0, \quad (3)$$

$$\text{with } \alpha = \frac{2}{\sqrt{\pi \kappa c_p \rho}},$$

where  $j$  is the net heat flux just below the water surface and  $t_0$  the time at which a surface renewal event occurred. The thermal diffusivity is indicated by  $\kappa$ , the specific heat by  $c_p$  and the density of seawater by  $\rho$ . Under conditions found frequently over the open ocean, the temperature difference

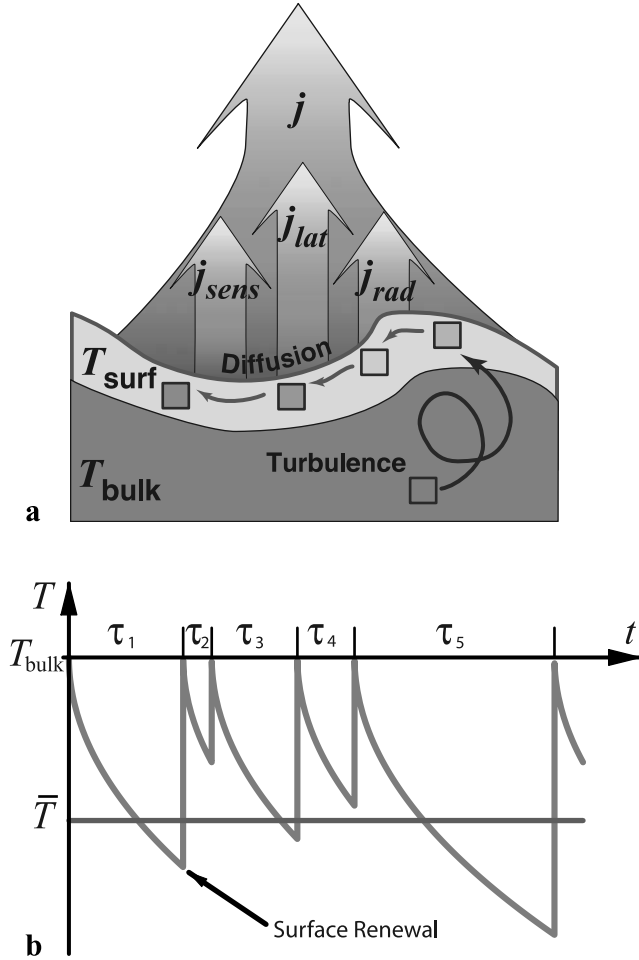


**Figure 1.** (a) Schematic drawing of the thermal boundary layer and the surface renewal model. (b) Illustration of the sea surface temperature  $T$  with respect to time  $t$ . See color version of this figure in the HTML.

across the thermal boundary layer  $\Delta T = T_{\text{bulk}} - T_{\text{surf}}$  is of the order of 0.1–0.3 K [Wick *et al.*, 1996].

[10] Affixed to the surface renewal model is the probability density function  $p(\tau)$  of times between consecutive surface renewal events. Following [Kraus and Businger, 1994], a probability density function (pdf)  $p(\tau)$  is defined which represents the fractional area of the surface fluid elements that have been in contact with the interface for a time  $\tau$ . From Taylor's theorem [Taylor, 1938],  $p(\tau)$  is of course equivalent to the probability of finding a surface renewal event taking place after the passing of time  $\tau$ .

[11] In literature two important, distinctly different expressions for the probability density function  $p(\tau)$  have been suggested. The first distribution for  $p(\tau)$  was introduced by Danckwerts [1951]. It is assumed that the turbulence in the interior of the fluid governs the mechanism for replacing the surface elements. This represents a random process and it is argued that each fluid element has the same probability of being replaced, which can be expressed as

$$\frac{dp(\tau)}{d\tau} = -\frac{1}{T_{\text{surf}}} p(\tau) \quad \text{leading to} \quad p(\tau) = \frac{1}{T_{\text{surf}}} \exp\left(-\frac{\tau}{T_{\text{surf}}}\right), \quad (4)$$

where  $T_{\text{surf}}$  is the characteristic residence time of fluid parcels at the surface.

[12] Kolmogorov [1962] and Soloviev and Schlüssel [1994] argue along the same line of reasoning but deduce a logarithmic normal distribution of the form

$$p(\tau) = \frac{1}{\sqrt{\pi}\sigma\tau/t'} e^{-\frac{(\ln\tau/t' - m)^2}{\sigma^2}}, \quad t > 0, \quad (5)$$

where  $m$  is the mean value of  $\ln \tau/t'$  and  $\sigma^2$  the variance for the logarithm of the scaled random variable  $\tau$ .  $t'$  is a unit scaling factor. The mean time between burst  $T_{\text{surf}}$  is the expectation value of this distribution, given by

$$T_{\text{surf}} = \langle p(\tau) \rangle = \int_0^{\infty} p(\tau)\tau/t' d\tau = t' \cdot e^{\frac{\sigma^2}{2} + m}. \quad (6)$$

The function of the sea surface temperature with respect to time for the logarithmic normal pdf is illustrated in Figure 1.

[13] This type of model pdf was indicated by measurements of Rao *et al.* [1971] and more recently of Garbe *et al.* [2001]. For this reason a surface renewal model with a logarithmic normal pdf is assumed in deriving the techniques presented in the following sections. Thus consistent results of these techniques with independent measurements present an indirect verification of this surface renewal model. This does of course also mean that the techniques presented are only applicable to conditions in which the model describes the transfer process. This excludes day time measurements, as well as conditions of the air water interface, strongly contaminated with surface active materials.

### 3. Cool Skin Temperature Difference

[14] Measuring the temperature difference across the thermal boundary layer invasively is a difficult undertaking because of thin layer extending less than 1 mm beneath the wavy interface. Combining model assumptions with a statistical analysis of the infrared imagery, this important parameter can be retrieved to an accuracy of less than 1% from modern IR cameras. The statistical analysis is based on fitting an analytical function to the temperature distribution at the sea surface. The analytical function can be derived from the surface renewal model, as is outlined in Appendix A. Here use is made of  $\Delta T$  given by equation (3) and the lognormal distribution of  $p(\tau)$  for surface renewal events. The temperature distribution at the sea surface  $p(T_{\text{surf}})$  is then given by

$$p(T_{\text{surf}}) = \mathfrak{S}(\text{sign}(j) \cdot \Delta T) \frac{|T_{\text{surf}} - T_{\text{bulk}}|}{(\alpha j)^2} \exp\left[\frac{\sigma^2}{4} - m\right] \cdot \text{erfc}\left[\frac{\sigma}{2} - \frac{m}{\sigma} + \frac{1}{\sigma} \ln\left(\frac{T_{\text{surf}} - T_{\text{bulk}}}{\alpha j}\right)\right]^2 \quad (7)$$

with  $\alpha = \frac{2}{\sqrt{\alpha \kappa \rho c_p}}$

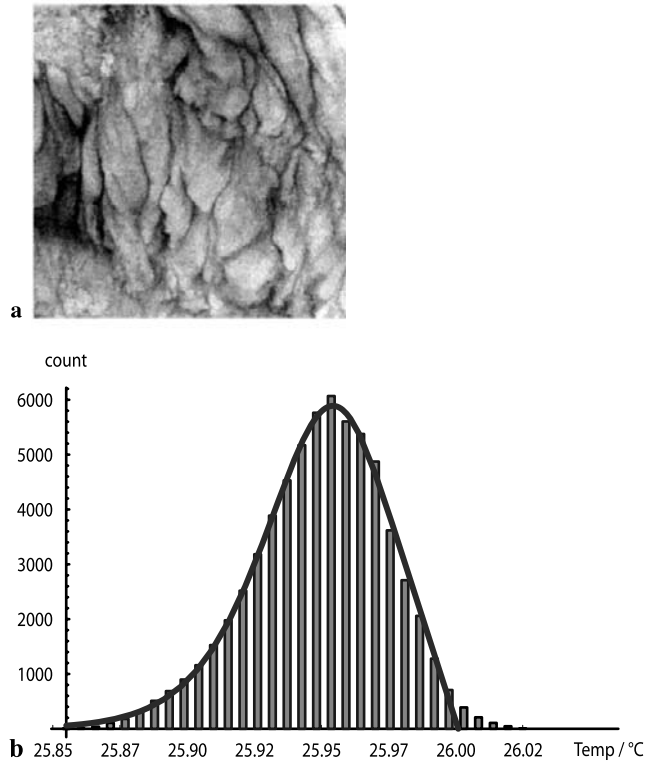


**Figure 2.** The analytical function describes the temperature distribution of the IR image shown in Figure 2a quite well, as can easily be verified from the fit in Figure 2b. See color version of this figure in the HTML.

for  $j \neq 0$  and  $p(T_{\text{surf}}) = \delta(\Delta T)$  for  $j = 0$  [Haußecker *et al.*, 2001]. Here  $\Delta T = T_{\text{surf}} - T_{\text{bulk}}$  denotes the temperature difference,  $\text{erfc}$  is the complementary error function,  $\delta(x)$  denotes Dirac's delta distribution,  $\text{sign}(x)$

the sign function and  $\mathfrak{S}(x)$  the Heaviside unit step function

$$\text{sign}(x) = \begin{cases} 1, & x \geq 0 \\ -1, & x < 0 \end{cases} \quad \text{and} \quad \mathfrak{S}(x) = \begin{cases} 1, & x \geq 0 \\ 0, & x < 0 \end{cases}. \quad (8)$$

The complementary error function is defined as  $\text{erfc}(z) = 1 - \text{erf}(z)$  and the error function given by the integral of the Gaussian distribution  $\text{erf}(z) = 2/\sqrt{\pi} \int_0^z \exp(-\eta^2) d\eta$ .

[15] From Taylor's hypothesis the analytical function for the probability density function  $p(T_{\text{surf}})$  can be fitted to the frequency density function of the temperature distribution from an individual image, as can be seen in Figure 2. This makes it possible to estimate the temperature of the bulk  $T_{\text{bulk}}$  with the frame rate of the IR camera. The mean temperature  $\overline{T_{\text{surf}}}$  at the sea surface is given as the expectancy value of the temperature distribution

$$\overline{T_{\text{surf}}} = \int_{-\infty}^{\infty} T_{\text{surf}} \cdot p(T_{\text{surf}}) dT_{\text{surf}}. \quad (9)$$

This integration can be solved numerically, resulting in a value for  $\overline{T_{\text{surf}}}$  that is much less prone to errors in the data than calculating  $\overline{T_{\text{surf}}}$  by just summing over the image intensities and dividing by the number of pixels. From the knowledge of both  $T_{\text{surf}}$  and  $T_{\text{bulk}}$  the temperature difference  $\Delta T = T_{\text{surf}} - T_{\text{bulk}}$  can be computed.

### 3.1. Interdependence of Parameter

[16] Even though the temperature of the bulk water  $T_{\text{bulk}}$  can be estimated from a statistical analysis of the temperature distribution of the sea surface, this frequency data does not hold enough information to independently estimate all parameters of the analytical function in equation (7). An illustration of the interdependence of the parameter  $m$  and the heat flux  $j$  is presented in Figure 3.

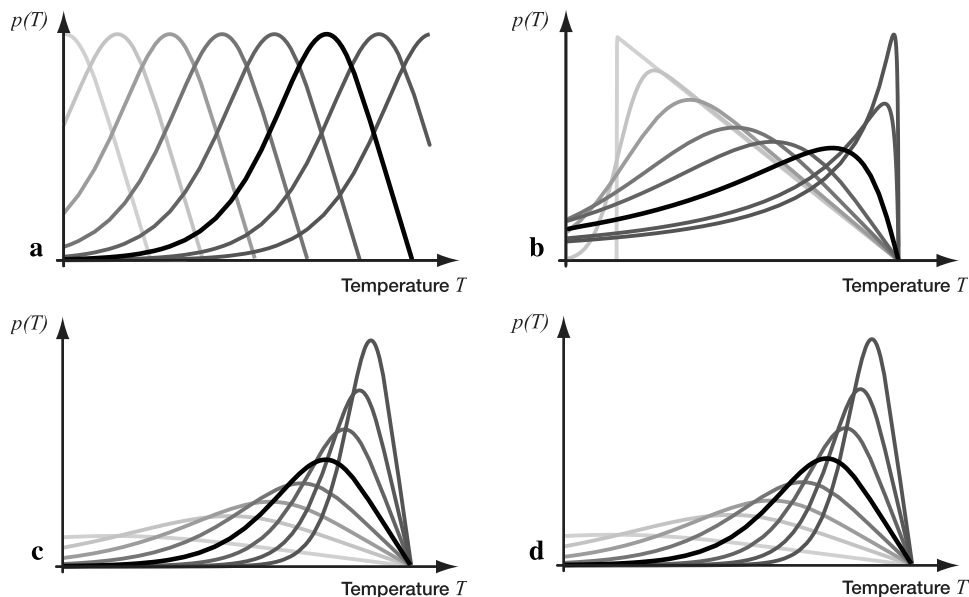


**Figure 3.** Plot of the probability density function  $p\tau$ . Both  $T_{\text{bulk}}$  and  $\sigma$  can be estimated independently from the fit, as is evident from the plots of (a) different  $T_{\text{bulk}}$  and (b) different values of  $\sigma$ . The values for  $j$  and  $m$  cannot be computed independently, as is apparent from the same plots for (c) different  $m$  and (d) different values of  $j$ . See color version of this figure in the HTML.

[17] The interdependence of the parameters  $m$  and  $j$  is expressed in the fact that the same analytical curve can be fitted for different values of  $m$  and  $j$ . This can easily be verified by analyzing equation (7). The terms in this equation can be divided into two groups, namely into terms that normalize the function and terms that are responsible for the general shape of  $p(T_{\text{surf}})$ . Equating both the shape and normalization terms for two values of  $m$  and  $j$  leads to a condition under which the same curve results for different values of  $j$  and  $m$ . This condition is given by

$$\left(\frac{j_2}{j_1}\right)^2 = e^{m_1 - m_2}. \quad (10)$$

It can in fact be shown by the same procedure, that the same histogram only results from different combinations of  $m$  and  $j$ , but not from other combinations of the parameters.

[18] Even though the parameters  $\sigma$ ,  $m$  and  $j$  can not be determined independently by the method described in this section, the bulk temperature  $T_{\text{bulk}}$  can be estimated accurately. As indicated by Figure 3,  $T_{\text{bulk}}$  represents the intersection of the function of equation (7) with the axis of abscissae, which is independent of the exact value of  $j$ ,  $\sigma$  and  $m$ .

### 3.2. Accuracy of Parameter Estimation

[19] In order to test the validity of results gained from the statistical analysis proposed in section 3, the effect of noise in the input data on the estimated parameters was examined on synthetic data in a Monte Carlo type analysis. The synthetic data was generated, presenting the same distribution of gray values as a thermal image of the sea surface. The relative errors in the fit parameters were analyzed under varying noise level of the input data. The results of this analysis is presented in Figure 4.

[20] By comparing the results it becomes apparent that the bulk temperature  $T_{\text{bulk}}$  can be estimated with a relative accuracy of below 1% for noise levels of 0.2 K. For the noise level of the infrared camera, typically 25 mK, the error in  $T_{\text{bulk}}$  was found to be well below 5 mK. This is in good agreement with previous findings on real data [Schimpf et al., 2004]. In contrast to the errors of the other parameters there is only a small increase with a rising noise level. It becomes evident that the errors in the parameter  $m$ ,  $\sigma$  and  $j$  rise very strongly with increasing noise level. However, in subsequent analyzes only the parameter  $T_{\text{bulk}}$  is used. Therefore the higher noise levels in the other parameters turn out not to be problematic. However, caution should be used if the other parameters  $m$  and  $\sigma$  are of interest. These can be retrieved more accurately by the analysis presented in section 6.

## 4. Image Sequence Analysis

[21] The technique of simultaneously estimating optical flow and change of image intensity, or, in the case of thermal images, temperature change, is well known in literature [Negahdaripour and Yu, 1993; Zhang and Herbert, 1999; Haußecker et al., 1999; Haußecker and Fleet, 2001]. Details of the technique employed in the context of this paper, including the estimation of local convergence and divergence, have been explained previously [Garbe et al.,

2003]. Accuracy improvements were introduced by Garbe and Jähne [2001] and Garbe et al. [2002]. Therefore only a brief overview of the technique shall be presented here.

[22] As will become apparent from the remainder of this paper, determining the total derivative of the sea surface temperature with respect to time is a vital prerequisite for estimating a number of parameters governing the atmosphere ocean heat transfer. This total derivative is given by  $dT/dt = \partial T/\partial t + \vec{u} \cdot \nabla T$ , where  $T$  is the sea surface temperature and  $\vec{u} = (u_1, u_2)^T$  the surface flow. This derivative can be formulated in vector notation, yielding

$$\vec{d}^T \cdot \vec{p} = (-1, T_x, T_y, T_t) \cdot (c, \delta x, \delta y, \delta t)^T = 0, \quad (11)$$

where the subscripts  $A_B$  denote partial derivatives of the variable  $A$  along the coordinate  $B$ . Here  $c$  is the parameter of linear temperature change. The transpose of a vector  $\vec{a}$  is indicated by  $\vec{a}^T$ . The total derivative  $dT/dt$  is then given by  $dT/dt = c/\delta t$  and the velocities by  $u = \delta x/\delta t$  and  $v = \delta y/\delta t$ .

[23] This equation poses an underdetermined system of equations as only one constraint is given for four unknowns. The problem can be solved by assuming constant parameters in a small spatiotemporal neighborhood. A typical neighborhood will usually range between  $n = 5 \times 5$  and  $n = 11 \times 11$  pixel. In this neighborhood one constraint of equation (11) is given per pixel, with an adequate weighting applied. Solving this overdetermined system of equations is performed in an error-in-variables model or total least squares, which essentially boils down to a singular-value analysis of the data matrix  $\mathbf{D}$  [Van Huffel and Vandewalle, 1991]. The accuracy can be improved by applying a mixed total least squares-ordinary least squares estimator [Garbe et al., 2002]. The results of this computation are shown in Figure 5.

[24] When dealing with thermal images from the sea surface, especially with field data, reflections from the surroundings are impossible to eliminate. Such reflections cannot be eliminated by a global threshold because their apparent temperature is very close to that of the thermal structures of the sea surface. However, they can be detected as outliers and segmented by a robust estimation of  $dT/dt$  [Garbe and Jähne, 2001], as is shown in Figure 6. Only through this step is an accurate estimation of  $dT/dt$  possible, as is the computation of  $T_{\text{bulk}}$  from the algorithm introduced in section 3.

## 5. Time of Residence at the Water Surface and Transfer Velocity of Heat

[25] As was pointed out previously the time of residence of a water parcel at the sea surface  $\tau = t - t_0$  is an important parameter in the model of surface renewal. From the definition of the transfer velocity in equation (1) it becomes apparent that  $\tau$  is equivalent to  $k_{\text{heat}}$ . This can be verified by inserting equation (3) into equation (1), leading to

$$k_{\text{heat}} = \frac{1}{\rho c_p \alpha \sqrt{\tau}} = \frac{1}{2} \sqrt{\frac{\pi \kappa}{\tau}}. \quad (12)$$

Through thermography  $\tau$  can be measured directly. From the assumption that  $k_{\text{heat}}$  is a well behaved function in space

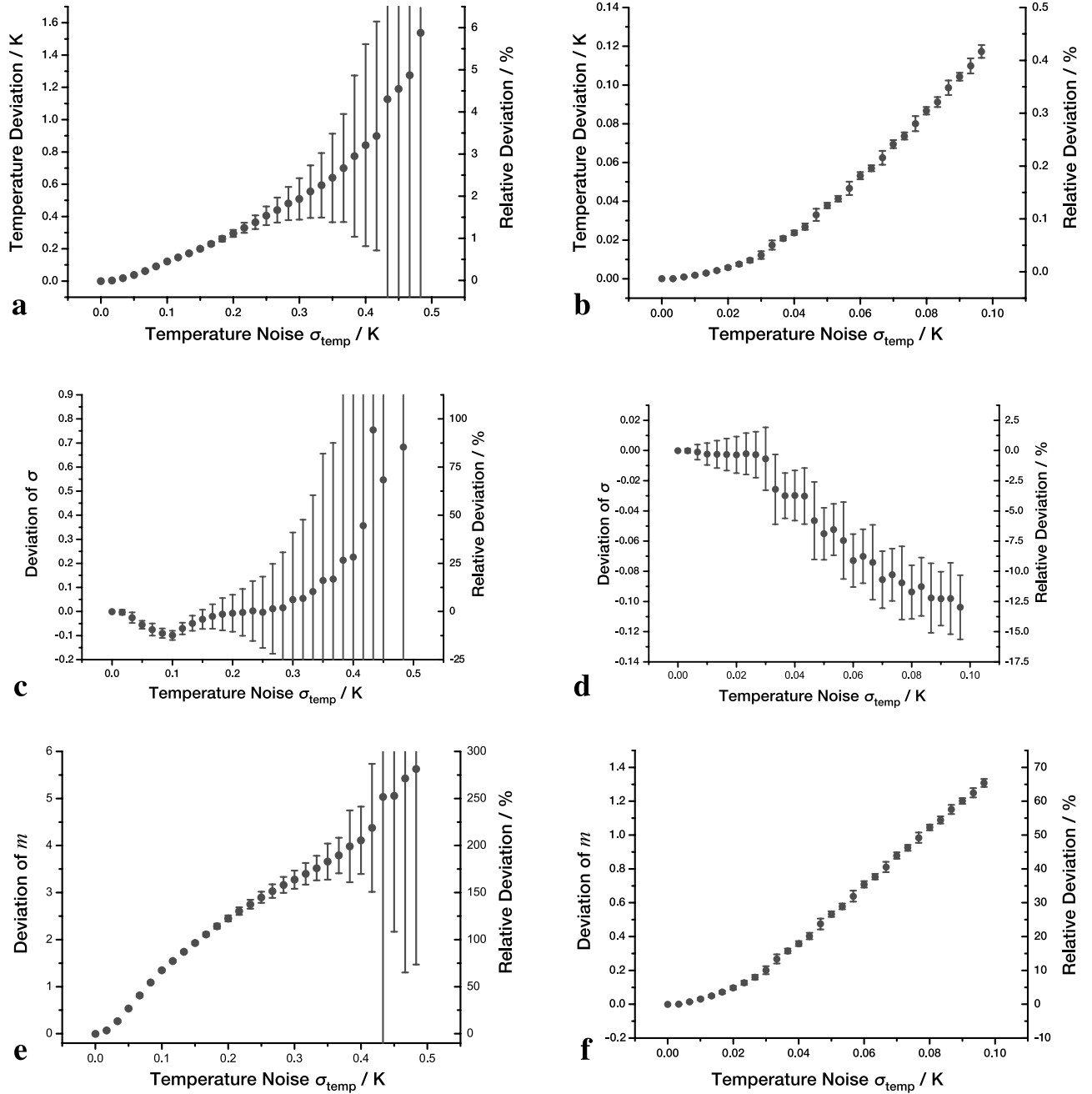


**Figure 4.** The dependence of the extracted parameters from the statistical analysis on the noise. (a) The dependence of the error of  $T_{\text{bulk}}$  on the noise ranging from 0.0 to 0.5 K is shown. (b) The same for lower noise levels from 0.0 to 0.1 can be seen. (c)–(f) The analogue for the error of the other parameters  $\sigma$  and  $m$  is given. See color version of this figure in the HTML.

and time, equation (12) states that the same holds true for  $\tau$ . This implies that  $\tau$  can be measured regardless of a slowly changing heat flux, since this would lead to a change in  $\Delta T$  and hence a constant  $k_{\text{heat}}$  and  $\tau$ .

[26] Reformulating equation (3) leads to an expression for  $\tau$ :

$$\tau = t - t_0 = \left( \frac{T_{\text{surf}}(t) - T_{\text{bulk}}}{\alpha j} \right)^2, \quad \text{with} \quad \alpha = \frac{2}{\sqrt{\pi k c_p \rho}}. \quad (13)$$

[27] In this equation the surface temperature  $T_{\text{surf}}$  is given directly by the temperature calibrated infrared

images. The bulk temperature  $T_{\text{bulk}}$  can either be measured with thermometers or from thermography as has been outlined in section 3. Measuring  $T_{\text{bulk}}$  from thermometers is an extremely difficult undertaking, as  $\Delta T$  is usually of the magnitude of 0.1 K and the boundary layer extends less than a one millimeter beneath the surface. Also, a thermal stratification may be present very close to the interface making the measurement of  $T_{\text{bulk}}$  dependent on the chosen depth and may thus lead to wrong results.

[28] Another problem in equation (13) is the measurement of the net heat flux  $j$ . This can be circumvented by

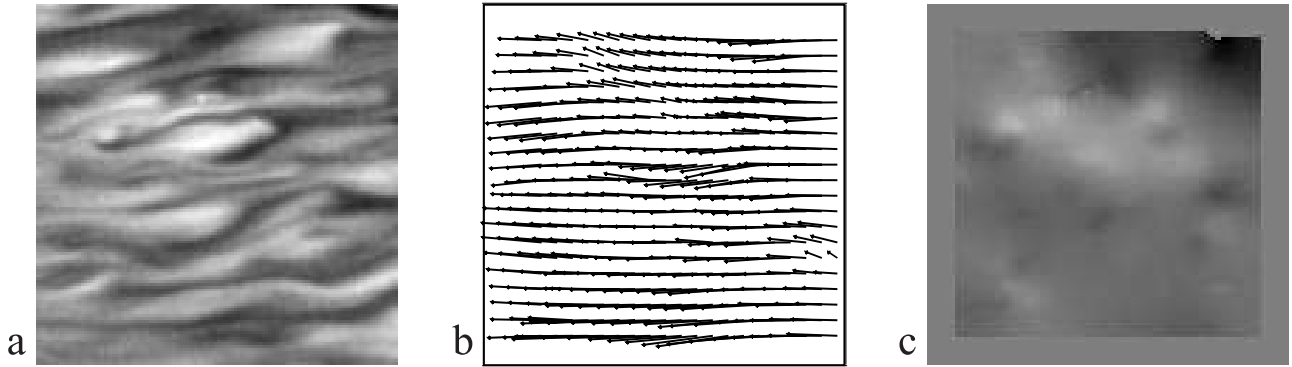


**Figure 5.** (a) An IR image is shown with (b) the corresponding 2-D optical flow and (c) the total derivative of the temperature ( $[-0.6, 0.4]$  K/frame).

differentiating equation (3) with respect to time and solving it for  $j$ . This leads to

$$j = \frac{2\sqrt{\tau}}{\alpha} \frac{d}{dt} T_{\text{surf}}(t). \quad (14)$$

By substituting equation (14) into equation (13) the following expression for  $\tau$  can be derived:

$$\tau = t - t_0 = \frac{1}{2} \frac{T_{\text{surf}}(t) - T_{\text{bulk}}}{\frac{d}{dt} T_{\text{surf}}(t)} = \frac{1}{2} \frac{\Delta T(t)}{\dot{T}_{\text{surf}}(t)}, \quad (15)$$

where in the dotted notation  $\dot{x}$  indicates the total derivative with respect to time.

[29] In this reformulation of the problem, only  $\Delta T$  and the total derivative  $d/dt T_{\text{surf}} = \dot{T}_{\text{surf}}$  have to be estimated from measuring  $\tau$ . Both these quantities can be estimated from thermography as has been shown in the preceding sections. It should be noted that  $\Delta T$  is computed for every pixel of the thermal image sequence as is  $\dot{T}_{\text{surf}}$ . Likewise  $\tau$  is estimated at every pixel, leading to a temporally and spatially highly resolved measurement limited only by the thermal imager.

[30] Once  $\tau$  is known from equation (15) for every pixel of the IR image sequence the transfer velocity  $k_{\text{heat}}$  follows from equation (12). This leads to

$$k_{\text{heat}} = \sqrt{\frac{\pi \kappa}{2}} \cdot \sqrt{\frac{\dot{T}_{\text{surf}}}{\Delta T}}. \quad (16)$$

[31] It is of course important to analyze possible errors in the estimation of both  $\tau$  and  $k_{\text{heat}}$  by the proposed technique. Assuming the errors in the estimation to be distributed according to Gaussian statistics, the deviation in the estimate can be derived by error propagation. This leads to the relative error given by

$$\frac{\sigma_{k_{\text{heat}}}}{k_{\text{heat}}} = \frac{1}{2} \frac{\sigma_{\tau}}{\tau} = \frac{1}{2} \sqrt{\left(\frac{\sigma_{\Delta T}}{\Delta T}\right)^2 + \left(\frac{\sigma_{\dot{T}_{\text{surf}}}}{\dot{T}_{\text{surf}}}\right)^2}. \quad (17)$$

In conditions typical for air-sea gas exchange the relative errors of  $\Delta T$  and  $\dot{T}_{\text{surf}}$  can both be approximated by

$\sigma_{\Delta T}/\Delta T \approx \sigma_{\dot{T}_{\text{surf}}}/\dot{T}_{\text{surf}} \approx 5\%$ . This leads to a relative error of about  $\sigma_{\tau}/\tau \approx 7.1\%$  and  $\sigma_{k_{\text{heat}}}/k_{\text{heat}} \approx 3.6\%$ .

## 6. Pdf of Surface Renewal From Thermography

[32] The pdf of surface renewal gives rise to speculations regarding the exact processes involved in the renewal events and justifies the statistical analysis of the sea surface temperature described in section 3 as well as some of the techniques in estimating the heat flux described later on.

[33] In order to be able to make a quantitative statement on this pdf, a statistical analysis on the time of residence  $\tau$  of water parcels at the water surface is performed. From equation (15) a value for  $\tau$  can be computed at every pixel. Given the theoretical lognormal  $p(\tau)$  from equation (5), the values for  $\sigma$  and  $m$  can be computed together with error estimates for the individual parameters. This is achieved by fitting  $p(\tau)$  to the histogram of  $\tau$  by means of least squares as can be seen in Figure 7. From the parameters  $\sigma$  and  $m$  the characteristic mean time between surface renewals  $T_{\text{surf}}$  can be computed from equation (6). This presents a powerful means of verifying the pdf of surface renewal.

## 7. Heat Flux Estimates

[34] In previous sections different techniques for estimating  $\Delta T$ ,  $\tau$  and  $k_{\text{heat}}$  noninvasively have been presented. Another important parameter for air-water heat exchange is the net heat flux  $j$ . The heat flux  $j$  for a substance of mass  $M$  is defined as the rate of change of heat  $Q$  across the surface area  $A$ , or

$$j = \frac{dQ/dt}{A} = \frac{Mc_p dT}{A dt}. \quad (18)$$

In the following two distinct methods for estimating the net heat flux from the surface renewal model in thermal image sequences will be presented.

### 7.1. Pdf Method

[35] This method may be used to compute the mean heat flux over part of the sequence. It is termed pdf method, as a statistical analysis of the times individual water parcels are resident on the water surface is performed. Evidently some assumptions have to be made in order to derive the net heat flux from this analysis. The

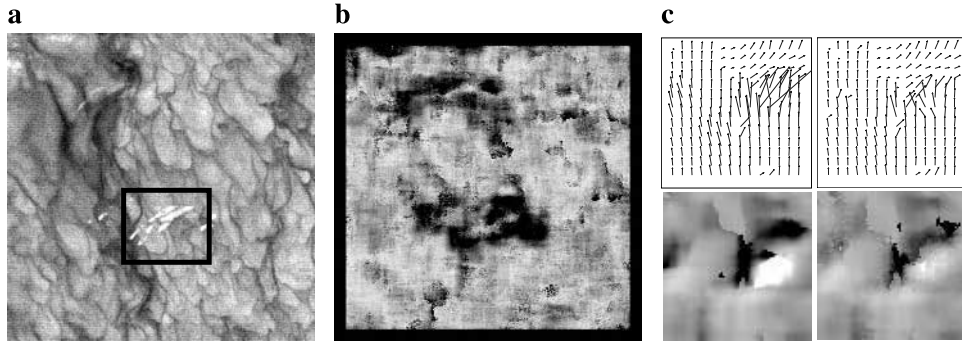


**Figure 6.** (a) An IR image, (b) the number of weights as computed by LMSOD. Black areas indicate fewer weights which corresponds to reflections. (c) The flow field and the total derivative  $dT_{\text{surf}}/dt$  inside the box in Figure 6a. Black regions indicate where no parameters could be estimated.

first one is of course that the surface renewal model as introduced in section 2 describes the transport processes sufficiently well. The other is that the pdf of the times of residence of the water parcels at the sea surface can be described by a lognormal distribution. As indicated in section 6, strong experimental evidence exist to make this a valid assumption. In section 7.2 another technique will be introduced which does not rely on any assumptions concerning the pdf of surface renewal. Comparing results of these two techniques can be seen as an indirect verification of the assumption concerning the pdf of surface renewal made by the pdf method.

[36] The average temperature difference across the cool skin of the ocean is given by *Soloviev and Schlüssel* [1994] as

$$\overline{\Delta T} = \int_0^{\infty} p(\tau)\tau^{-1} \left( \int_0^{\tau} \Delta T(t') dt' \right) d\tau. \quad (19)$$

The integration of this equation with the lognormal pdf from equation (5) and the expression for  $\Delta T$  from equation (3) yields

$$\overline{\Delta T} = \frac{2}{3} \alpha j \sqrt{T_{\text{surf}}} \exp(-\sigma^2/16) \quad \text{with} \quad \alpha = \frac{2}{\sqrt{\pi \kappa c_p \rho}}. \quad (20)$$

This expression can be solved for the heat flux  $j$ , which together with equation (6) for  $T_{\text{surf}}$  leads to

$$j = \frac{3 \overline{\Delta T}}{2 \alpha} \cdot \exp \left[ - \left( \frac{\sigma^2}{16} + \frac{m}{2} \right) \right]. \quad (21)$$

Both parameters  $\sigma$  and  $m$  can be computed from the pdf of surface renewal as outlined in section 6.

## 7.2. Square Root Method

[37] As opposed to the pdf method outlined in the previous section this technique does not rely on assumptions concerning the pdf of times between consecutive surface renewal events  $p(\tau)$ . Use is made only of the surface renewal model introduced in section 2 for deriving this method. This makes the square root method very well suited for estimating the net heat flux  $j$ .

[38] The surface renewal model introduced in section 2 yields equation (3) for  $\Delta T$ . Solving this equation for the heat flux  $j$  and making use of equation (15) for  $\tau$  leads to

$$|j| = \frac{\sqrt{2}}{\alpha} \sqrt{\Delta T \cdot \frac{d}{dt} T_{\text{surf}}(t)}. \quad (22)$$

The sign of the heat flux  $j$  in equation (22) is affixed to a heating up or cooling down of water parcels at the sea surface. Therefore it can be deduced from the sign of the total derivative  $dT_{\text{surf}}/dt$ , or  $\text{sign}(j) = \text{sign}(dT_{\text{surf}}/dt)$ .

[39] For specifying the error bounds of the square root method, errors can be assumed to be Gaussian distributed. Error propagation then leads to the relative error given by

$$\frac{\sigma_j}{j} = \frac{1}{2} \sqrt{\left( \frac{\sigma_{\Delta T}}{\Delta T} \right)^2 + \left( \frac{\sigma_{\dot{T}_{\text{surf}}}}{\dot{T}_{\text{surf}}} \right)^2}. \quad (23)$$

The relative error of both  $\Delta T$  and  $\dot{T}_{\text{surf}}$  are typically of the order of  $\sigma_{\Delta T}/\Delta T \approx \sigma_{\dot{T}_{\text{surf}}}/\dot{T}_{\text{surf}} \approx 5\%$ . Thus  $\sigma_j/j \approx 3.6\%$  should be achievable for  $j$ .

[40] In general conditions of interest for air-sea gas exchange, net heat fluxes during the night will be of around  $j \approx 200 \text{ W/m}^2$ . With a relative error of 4% the absolute error would be  $\sigma_j = 8 \text{ W/m}^2$ . This is within the bounds of errors

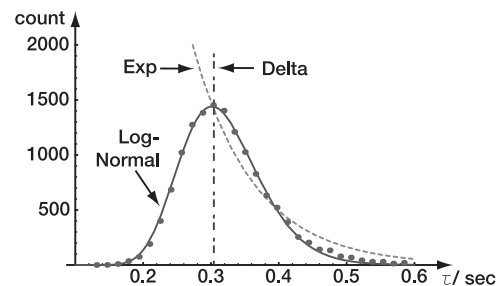


**Figure 7.** The frequency data of the time of residence  $\tau$  of a water parcel at the sea surface. The fitted lognormal distribution approximates the data quite well. Fitted are also exponential and delta distribution. The data points were computed from one sequence of the GasExII data. See color version of this figure in the HTML.

the TOGA CORE experiment tried to achieve [Fairall *et al.*, 1996b].

## 8. Assumptions and Limitations

[41] The techniques for measuring the parameters  $\Delta T$ ,  $\tau$ ,  $k_{\text{heat}}$  and  $j$  rely on the surface renewal model described in section 2. All models present some form of simplification of the actual processes under consideration and this model presents no exception. Simplifications and restrictions inherent to the model will obviously also limit the techniques derived from it. Hence a closer look at the model assumptions is important in evaluating the validity of the methods proposed.

[42] The fundamental model assumption is that the heat transfer at the sea surface can be described by the surface renewal model. This implies that  $\Delta T$  can be calculated according to equation (3) by assuming spatial homogeneity tangential to the sea surface and thus reducing the problem to a one-dimensional one, orthogonal to the interface. Furthermore a constant flux boundary condition is assumed at the sea surface. The question then is, if these two assumptions are justified and inherently prohibit temporally and spatially highly resolved measurements.

[43] It should be noted that the proposed techniques for measuring the parameters of air-sea heat transport are estimated individually at each pixel of an thermal image sequence. As stated earlier, the resolution of current IR cameras and thus that of  $\tau$ ,  $k_{\text{heat}}$  and  $j_{\text{root}}$  is  $1.5 \times 1.5 \text{ mm}^2$  spatially and 10 ms temporally. It is safe to assume that  $j$  is a well behaved function of both space and time. This means that  $j$  varies smoothly and can be approximated by a Taylor series expansion. Because of the small scales of the measurements,  $j$  can be described fairly precisely by the leading order of the Taylor series. It can thus be considered constant at the small space and timescales. This argument is of course invalid if either the spatial or temporal resolution of the measurements were to be reduced.

[44] Besides the model of surface renewal the estimation of  $\Delta T$  relies also on the assumption of a well mixed bulk with constant temperature  $T_{\text{bulk}}$ . It is a well known fact that coherent structures persist close to the boundary of a wind driven sea, such as Langmuir circulations [Leibovich, 1983]. Depending on their magnitude, these coherent structures extend from centimeters to meters below the surface. Through these circulations the homogeneous distribution of temperature in the bulk might be altered. The technique presented in section 3 considers  $T_{\text{bulk}}$  to be present in a depth just below the thermal boundary layer. This is usually the depth of about 1 mm. Also, a constant bulk temperature is assumed for one frame of the IR image, thus extending  $40 \times 40 \text{ cm}^2$  spatially and 10 ms temporally. Current observations [Plueddemann *et al.*, 1996] and numerical simulations [McWilliams *et al.*, 1997] are concerned with Langmuir circulations extending from a few meters to a few hundred meters. Although first steps have been undertaken in resolving smaller scales [Melville *et al.*, 1998], it is not clear how big an effect coherent structures might have on the small scales of the footprint of the IR camera. Since no adverse effects were seen in our data it seems safe to

assume that the model assumption of a constant  $T_{\text{bulk}}$  over the image area is justified.

## 9. Experimental Setup

[45] The techniques presented in this work are passive techniques as no active elements such as lasers are needed for heating up patches of water. The experimental setup is thus much simpler than of active techniques [Haußecker, 1996]. However, because the temperature structures at the air-water interface are minute, great experimental care has to be taken not to obscure the investigated processes.

[46] Central to the experimental setup is an infrared camera. In recent years commercial camera systems have become readily available. They provide high frame rates and low noise levels. However, in the present context the temperature differences to be analyzed are in the range of 0.01–0.3 K and thus close to the noise level of modern cameras, which is typically 25 mK. The same holds true for the frame rate, as surface drift and wave motion is significant at higher wind speeds, calling for higher sampling rates to circumvent motion blurring or problems due to Shannon’s sampling theorem. In this respect the techniques presented here would improve immensely from imaging devices with even lower noise levels and higher frame rates.

[47] In experiments conducted at the Heidelberg wind-wave facility (the Aeolotron), an Amber Radiance 1 camera was used. For field experiments during the GasExII cruise thermographic image sequences were acquired with an Amber Galileo MWIR camera. Both cameras are based around a Stirling cooled InSb detector made up of a square  $256 \times 256$  focal plane array. The sensor is sensitive in a wavelength window of 3–5  $\mu\text{m}$ . The frame rate of the cameras is 60 Hz and 120 Hz for the Radiance and Galileo camera, respectively. The integration times were chosen between 1.3 and 1.9 ms, depending on the temperature of the water body. Longer integration times tend to exhibit a better signal-to-noise ratio while increasing the danger of overflows occurring in the image.

[48] To avoid strong reflections at the sea surface, the cameras in both field and laboratory experiments are mounted at an angle of about  $60^\circ$  to the mean sea surface. Illustrations of the setup for laboratory and field measurements are presented in Figure 8.

## 10. Laboratory Experiments

[49] Laboratory measurements were conducted at the Heidelberg Aeolotron, a dedicated circular wind wave facility. Wind speeds of up to 15 m/s can be attained by a rotating fiber glass enforced paddle ring. To allow precise heat flux measurements the walls of the Aeolotron are insulated by a 9 cm thick layer of Styrodur<sup>TM</sup> and are coated with a highly reflective aluminum foil in the air space. This ensures that the heat is transported predominantly through the water surface and not through the walls of the facility.

[50] In order to vary the heat flux the temperature of the water body can be increased by a 15.2 kW heating system. The air space is controlled by a closed loop air conditioning system with independent control of humidity and air temperature. High positive and negative heat fluxes at the water interface of more than  $1 \text{ kW/m}^2$  are achievable by  $64.1 \text{ kW}$

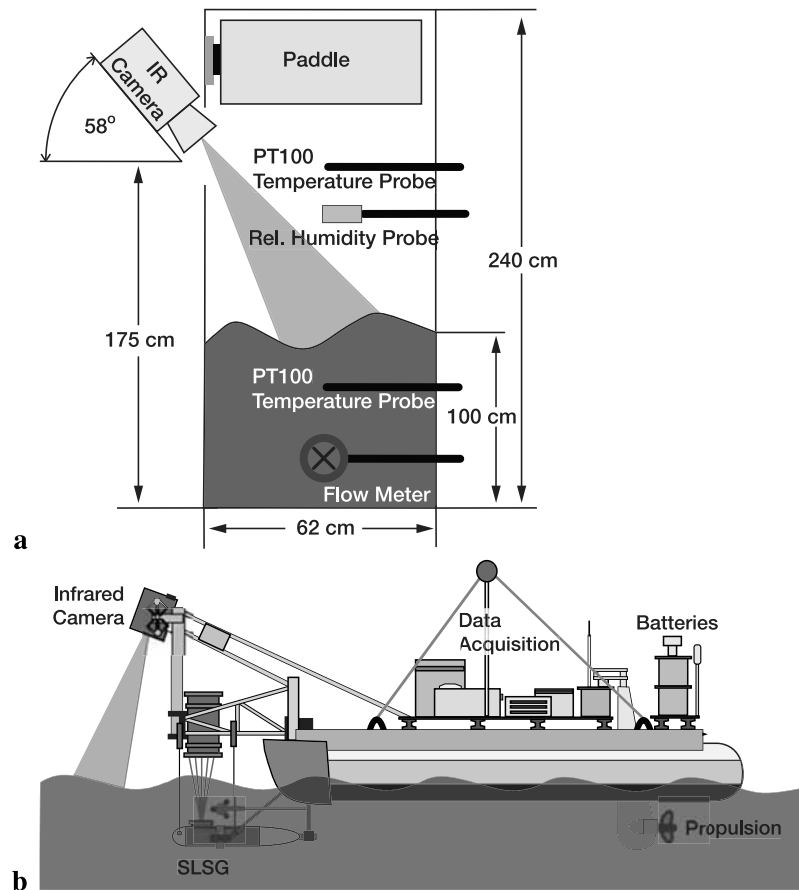


**Figure 8.** (a) A schematic cross section of the Heidelberg Aeolotron can be seen. An infrared camera images a  $(40 \times 40) \text{ cm}^2$  area of the water surface, with an angle of incidence of about  $30^\circ$ . (b) A drawing of the LADAS catamaran as used during the GasExII experiment. See color version of this figure in the HTML.

cooling and 15.6 kW heating capacity of the gas space. The specifications of the Aeolotron are given in Table 1.

### 10.1. Measurements of $\Delta T$

[51] The temperature difference  $\Delta T$  can be measured in the Aeolotron in two ways. In the context of this work the most important technique is obviously computing  $\Delta T$  from the statistical analysis of the infrared imagery as outlined in section 3. The reason is that only this analysis is equally applicable to the sea surface in field measurements. Also,  $\Delta T$  is estimated with the same device as the other parameters of heat exchange, resolving cross calibration issues.

[52] Another way of measuring  $\Delta T$  can be conducted by intermittently switching the net heat flux  $j$  on and off. In the experiments the net flux is given by the latent heat flux, since the sensible heat flux is zero because of the same air and water temperatures as is the radiative heat flux due to the reflective coating of the walls of the Aeolotron. A typical plot of water temperatures and relative humidity for such an experiment is presented in Figure 9. In the absence of a net heat flux the cool skin equilibrates and the surface temperature  $T_{\text{surf}}$  is equivalent to the bulk temperature  $T_{\text{bulk}}$ . This leads to a homogeneous image in the infrared camera of the bulk temperature  $T_{\text{bulk}}$ . In the presence of a net heat flux  $j$  the thermal boundary layer develops and the surface temperature  $T_{\text{surf}}$  is different from

that of the bulk  $T_{\text{bulk}}$ . The temperature difference  $\Delta T = T_{\text{surf}} - T_{\text{bulk}}$  can be computed from the images acquired during flux and no flux conditions, taking a steady decline of  $T_{\text{bulk}}$  due to  $j$  into account. An extensive analysis of this method has been performed by Schimpf *et al.* [2004] for different wind speeds with and without a surfactant. The results of this method for estimating  $\Delta T$  were compared to the one from the statistical analysis introduced in section 3. Both methods were in excellent agreement at all wind speeds examined, ranging from 1.2 m/s up to 6.1 m/s. It was shown that the statistical analysis presents a strong bias toward lower estimates at low wind speeds in the presence

**Table 1.** Key Technical Data of the Heidelberg Aeolotron

Property	Value
Channel height	2.407 m
Channel width	0.616 m
Inner radius	4.241 m
Outer radius	4.958 m
Mean circumference	29.217 m
Volume of channel	44.68 m <sup>3</sup>
Water surface area	18.00 m <sup>2</sup>
Nominal water depth	1.15 m
Nominal water volume	20.70 m <sup>3</sup>
Maximal wind speed	15 m/s

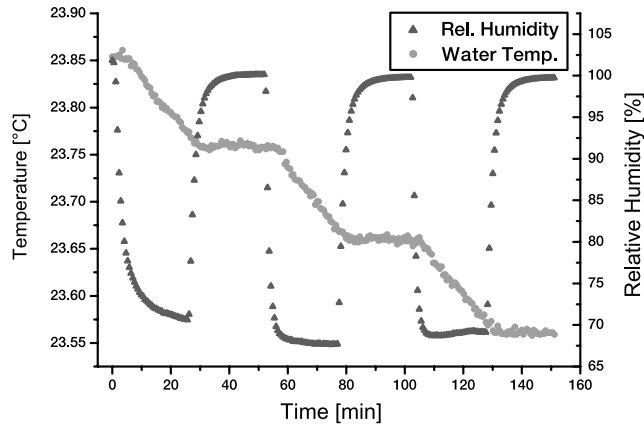


**Figure 9.** The water temperature and the relative humidity of the experiment conducted at a wind speed of 4.2 m/s. See color version of this figure in the HTML.

of surface slicks. This was attested to a damping of turbulence due to the surface film [Schimpf *et al.*, 2004].

[53] An error analysis of this method for calculating the temperature difference on synthetic data has been presented in section 3.2. It was shown that an accuracy of less than 3 mK can be expected, a value well in agreement with the empirical findings by Schimpf *et al.* [2004]. The values estimated for the temperature difference for three experiments are presented in Table 2.

## 10.2. Measurements of Heat Transfer

[54] The main purpose of the measurements conducted in the Heidelberg Aeolotron was to test the validity of proposed algorithms of estimating the net heat flux  $j$  at the sea surface. In that respect the different techniques of estimating  $j$  had to be compared to each other, as well as to a ground truth measure of the flux. Only through this analysis can the confidence bounds for the techniques be established as well as the limitations revealed.

### 10.2.1. Ground Truth of Net Heat Flux

[55] The Heidelberg Aeolotron is equipped with a Prema™ 3040 high precision thermometer collecting data from eight calibrated PT100 sensors in the water body. The precision of this thermometer is specified to 0.001 K with an accuracy of measurements with the PT100 elements of 0.004 K [Prema, 2000]. Thus the temperature change of the bulk water can be measured, which is directly related to the net heat flux. The ground truth data for the heat flux  $j_{\text{true}}$  can be computed from equation (18) and compared to the results estimated by the proposed algorithms.

[56] From error propagation the accuracy of the ground truth is found to be

$$\frac{\sigma_j}{j} = \sqrt{\left(\frac{\sigma_h}{h}\right)^2 + \left(\frac{\sigma_{dT/dt}}{dT/dt}\right)^2}. \quad (24)$$

**Table 2.** Results of the Heat Flux Measurements<sup>a</sup>

Wind Speed, m/s	$u_{*s}$ , m/s	$\Delta T$ , K	$j_{\text{true}}$ , $\text{Wm}^{-2}$	$j_{\text{pdf}}$ , $\text{Wm}^{-2}$	$j_{\text{sqr}}$ , $\text{Wm}^{-2}$	$t_{*s}$ , s
2.0	0.23	$0.140 \pm 0.003$	$-111 \pm 3$	$-124 \pm 11$	$-118 \pm 7$	$5.81 \pm 0.05$
4.2	0.66	$0.100 \pm 0.004$	$-163 \pm 2$	$-162 \pm 11$	$-165 \pm 14$	$1.82 \pm 0.03$
8.0	1.45	$0.053 \pm 0.003$	$-304 \pm 3$	$-273 \pm 23$	$-280 \pm 22$	$0.34 \pm 0.04$

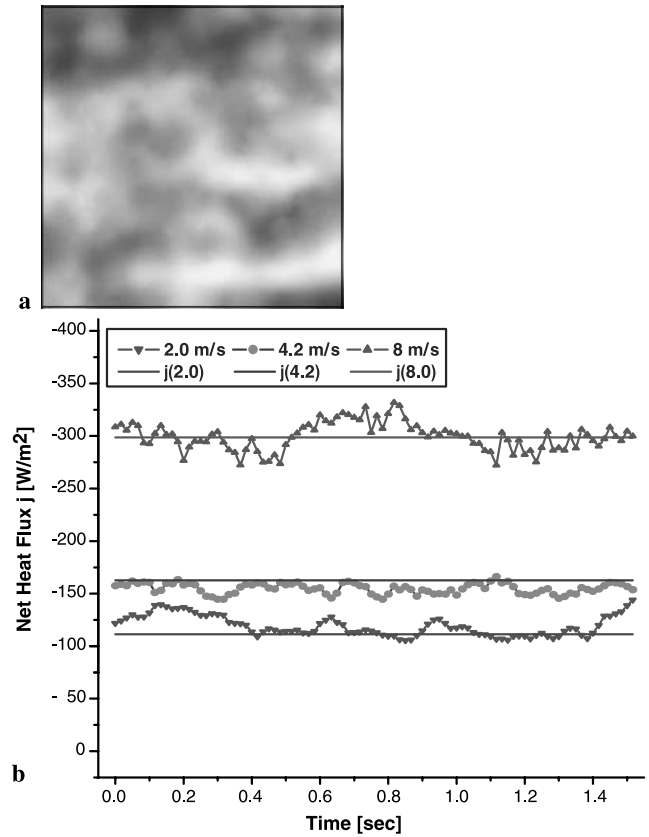


**Figure 10.** (a) An image of the estimated net heat flux. Bright areas indicate strong fluxes  $[-130, -100] \text{ W/m}^2$ . (b) The mean of the net heat flux computed from every frame for one sequence. See color version of this figure in the HTML.

The temperature decline  $dT/dt$  is estimated from linear regression by fitting a line with intersect ( $y = ax + b$ ) to the part of the data, where a constant heat flux is present. The fit can be performed to a relative accuracy of less than 1% and the measurement of the water height in the Aeolotron is performed with an acoustic measuring device, with a relative accuracy much better than that. The total relative accuracy of the net heat flux measured this way is thus equally better than 1%.

[57] For an accuracy evaluation of the proposed algorithms only the net heat flux through the air-water boundary is of interest. The residual transport of heat through the walls of the facility are computed from equation (18) during times devoid of an air-water interfacial heat flux. The flux measured this way was found to be below  $0.48 \text{ Wm}^{-2}$  during all experiments conducted. Fluxes of this magnitude are of the order of accuracy for the ground truth measurement and thus negligible. The values of  $j_{\text{true}}$  estimated from

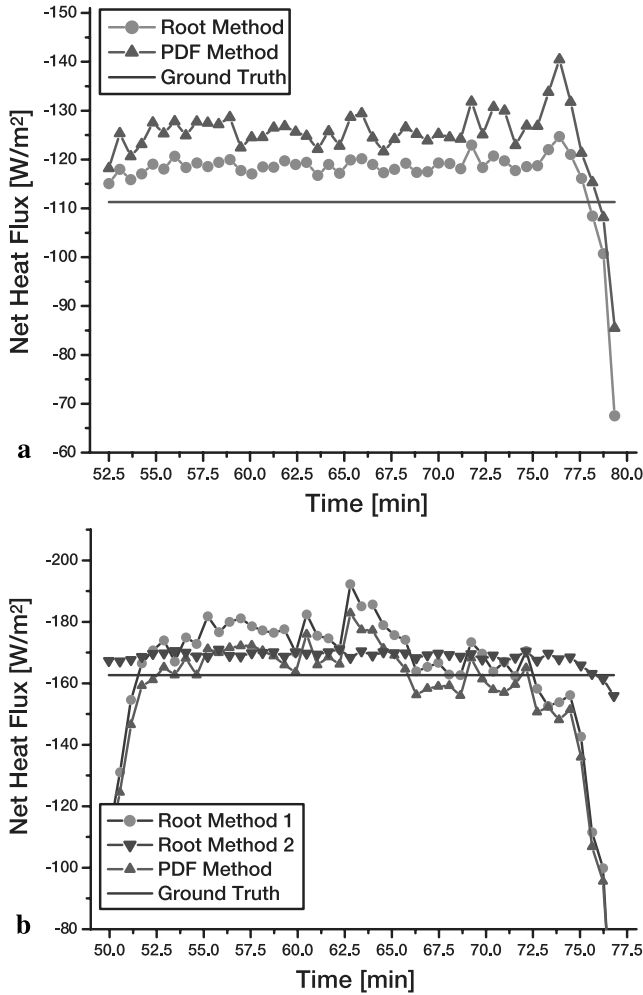


**Figure 11.** Heat flux estimate for wind of (a) 2 m/s and (b) 4.2 m/s. Shown are the results from the pdf method  $j_{pdf}$  and the square root method  $j_{root}$ , as well as the ground truth value  $j_{true}$ . Figure 11b,  $j_{root}$  was computed with the value of  $\Delta T$  estimates from the corresponding sequence (method 1) and also with the same mean value  $\overline{\Delta T}$  from all the sequences (method 2). See color version of this figure in the HTML.

the technique introduced in this section are presented in Table 2.

### 10.2.2. Thermographic Measurements

[58] Both the pdf method introduced in section 7.1 and the square root method presented in section 7.2 were used for computing the net heat flux in the experiments. As stated earlier the square root method is the preferred technique for it is not statistical in nature. Apart from making fewer assumptions on the nature of the heat transfer process, only this approach makes both spatially and temporal highly resolved estimates possible.

[59] The pdf of times between surface renewal events was computed following section 6. Under all conditions analyzed the estimated data followed the logarithmic normal distribution from equation (5) very well. The parameters  $\sigma$  and  $m$  computed from the fit of the distribution to the data is presented in Table 3. Also shown in this table is  $t_*$  which can be computed from  $\sigma$  and  $m$  as presented in equation (6).

[60] The good agreement of the data with a lognormal distribution makes the approach of the pdf technique for estimating the net heat flux seem valid. The results obtained from the pdf method as compared to the ground truth net heat flux is thus another verification of this assumption. It is of course much more indirect than fitting the distribution to the data of  $\tau$  as shown in section 6.

[61] Results of the square root technique are presented in Figure 10 for one image sequence and in Figure 11 for a measurement of 20 min. Shown is the high spatial resolution for  $j_{root}$  of less than  $3 \text{ mm}^2$ . The accuracy of the technique can also be seen in a sequence in which the mean heat flux estimated from individual images is shown and compared to the ground truth heat flux  $j_{true}$ . It should be noted that the temporal resolution is the frame rate of the infrared camera, which was 60 Hz in the measurements conducted in the Aeolotron. The fluctuations in the estimate are not due to errors but seem to be undulated because of waves passing through the imaged area.

[62] Presented in Figure 11 is the resulting heat flux estimate during the time of low relative humidity in the Aeolotron. Shown are the heat fluxes computed from both the square root method and the pdf method, as well as the ground truth value. The values shown are means derived from 90 images. The sudden decrease in the heat flux at the end of the measurements is due to the air conditioning system being turned off, leading to a sharp rise in relative humidity, which in turn causes the heat flux to terminate.

[63] Deviations in the estimate are largely due to fluctuations in the estimation of the temperature difference  $\Delta T$ . This is evident from Figure 11b where the heat flux was computed using the square root method with the estimated value for  $\Delta T$  from every single sequence and with the mean value for  $\Delta T$  from all the sequences. The estimate with the same value for  $\Delta T$  hardly fluctuates at all.

[64] In Table 2 the mean estimates of the net heat fluxes  $j_{root}$  and  $j_{pdf}$  for experiments at different wind speeds are presented. It is evident that both the estimates  $j_{root}$  and  $j_{pdf}$  are very close in accuracy. However, there seems to be a bias for the pdf method at low wind speeds toward higher values, whereas it seems to be closer to the ground truth  $j_{true}$  at higher wind speeds as compared to  $j_{root}$ . Overall both estimates seem to be closer to the true value in stronger winds than in the low wind speed case of 2 m/s. An explanation for this wind speed dependence is the applicability of the surface renewal model. In low wind speeds, the transport is driven by buoyancy while it is driven by shear in higher wind speed. Since the surface renewal model describes the shear driven transport better, the results are more accurate in this regime. This is even more true for the pdf method which not only assumes the surface renewal model but also a lognormal pdf. Hence the stronger bias of  $j_{pdf}$  in lower wind speeds. Also, the presence of adventitious films in the Aeolotron become more important at the low wind speeds. Again, these films lead to changes in the

**Table 3.** Results of the Statistical Analysis

Wind Speed, m/s	$\sigma$	$m$	$t_*$ , s
2.0	$0.62 \pm 0.02$	$1.65 \pm 0.003$	$5.81 \pm 0.05$
4.2	$0.61 \pm 0.02$	$0.50 \pm 0.02$	$1.82 \pm 0.03$
8.0	$0.37 \pm 0.02$	$-1.10 \pm 0.09$	$0.34 \pm 0.04$

**Table 4.** Results of the Heat Transfer Velocity  $k$  Measurements<sup>a</sup>

Wind Speed, m/s	$u_*$ , m/s	$k_{pdf}$ , cm/h	$k_{root}$ , cm/h	$k_{600,pdf}$ , cm/h	$k_{600,root}$ , cm/h	$k_{600,N_2O}$ , cm/h
2.0	0.23	76 ± 7	72 ± 4	3.64 ± 0.34	3.45 ± 0.19	2.65
4.2	0.66	139 ± 9	142 ± 12	14.24 ± 0.92	14.55 ± 1.23	10.09
8.0	1.45	443 ± 37	454 ± 36	45.38 ± 3.79	46.50 ± 3.69	42.23

<sup>a</sup>The Prandtl number  $Pr = 6.295$  and Schmidt number exponent  $n = 0.5$  were used, except for the measurement of 2.0 m/s wind speed

transport processes of heat, which are not modeled accurately by surface renewal.

[65] The heat transfer velocity was computed according to equation (16). Thus it is computed both spatially and temporally highly resolved. For comparison the transfer velocity for  $N_2O$  was measured from mass balance techniques (R. Nielsen, manuscript in preparation, 2004). For comparison the transfer velocities were scaled to a Schmidt number of  $Sc = 600$  following equation (2). The values of the transfer velocities estimated for the different experiments are presented in Table 4. These estimated values are plotted against the friction velocity  $u_*$  in Figure 12 (Table 4).

[66] It becomes apparent that the transfer velocities of heat are higher than the measurements for  $N_2O$  by a factor of roughly 30%. This discrepancy is higher than what is expected from the error analysis of the technique. In order to resolve this discrepancy further measurements under a range of different wind and surfactant conditions are required and will be conducted in the future.

## 11. In Situ Measurements

[67] The techniques presented in this work have been successfully employed in laboratory conditions. As shown in the previous section, in the Heidelberg Aeolotron a precise comparison of the estimated values for the net heat

flux and other parameters to the actual fluxes was possible. In this section we will show the applicability of the technique and some results of measurements during the GasExII experiment.

### 11.1. Measurements of $\Delta T$

[68] The statistical analysis introduced in section 3 was used to estimate the temperature difference  $\Delta T$  during the GasExII cruise. The values computed for  $T_{surf}$ ,  $T_{bulk}$  and the corresponding  $\Delta T$  can be seen in Figure 13 for one individual sequence. Also shown are the results of the estimation  $\Delta T$  for a typical deployment. The results for the deployments on year day 52, 54, 58 and 59 are shown in Figure 14. The temperature difference estimated from meteorological data is also presented for the same deployment. It is a striking feature that the method of estimating  $\Delta T$  from the infrared images is lower than the estimate from the meteorological data by 0.1–0.2 K. This is of course a significant difference in the estimates.

[69] It should be noted that the value for  $\Delta T$  estimated from meteorological measurements has not been assessed directly from temperature measurements. Moreover it has been computed from bulk parameterization of Fairall *et al.* [1996a]. In a recent experiment [Ward and Redfern, 1999] measured  $\Delta T$  directly and compared their findings to the predictions of different bulk parameterizations. They found discrepancies in the order of 0.05–0.2 K with a standard

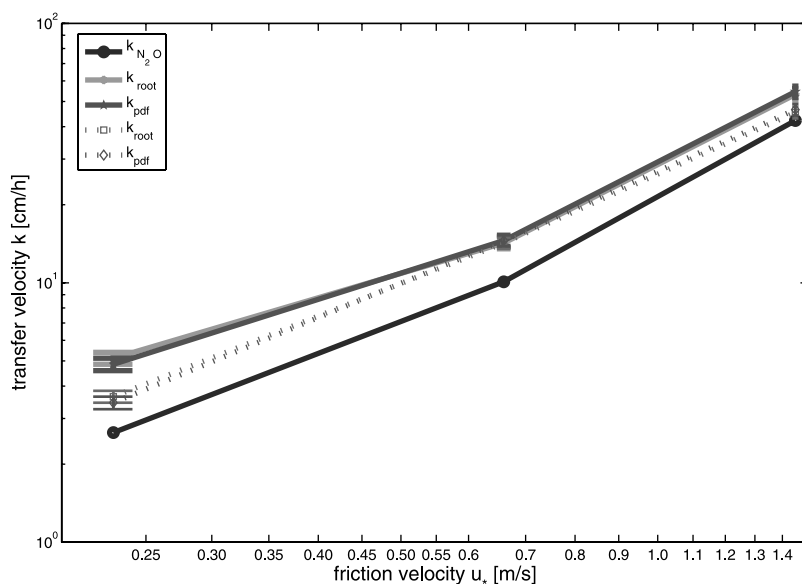


**Figure 12.** The laboratory measurements of the heat transfer velocity  $k_{600}$  computed from  $k_{heat}$  and  $k_{N_2O}$ . The transfer velocities are plotted against  $u_*$  in a log-log scale graph. See color version of this figure in the HTML.

**Table 5.** Results of the Statistical Analysis of the Renewal Process

Year Day	Wind Speed, m/s	$u_{*}$ , m/s	$\sigma$	$m$	$t_{*}$ , s
52	5.23	0.199	$0.51 \pm 0.02$	$0.06 \pm 0.06$	$1.08 \pm 0.05$
54	4.18	0.154	$0.46 \pm 0.02$	$-0.77 \pm 0.02$	$0.49 \pm 0.03$
58	5.05	0.184	$0.48 \pm 0.02$	$-0.28 \pm 0.02$	$0.83 \pm 0.05$
59	4.76	0.179	$0.56 \pm 0.02$	$0.67 \pm 0.03$	$2.13 \pm 0.04$

deviation in between 0.079 and 0.098 K and a bias ranging from 0.003 to 0.037 K between prediction and measurement, depending on the parameterization.

[70] The values for  $\Delta T$  could not be compared to other measurements. The model is only applicable to nocturnal measurements meaning that LADAS was deployed shortly after sunset. Because of day time solar irradiation it is to be expected that a temperature stratification in the bulk of the water was present. Because of the diffusion process it will take the stratification in the bulk much longer to clear away than the processes in the thermal boundary layer. A comparison will need to be much better than 0.05 K, which can hardly be achieved under stratified conditions, not even taking instrument cross calibration issues into account. In order to analyze the discrepancy between the IR technique and current invasive measurements, further experiments are necessary.

## 11.2. Measurements of Heat Transfer

[71] An important parameter for the model of surface renewal is the probability density function of times between consecutive surface renewal events. As has been presented in the previous section, the assumption of a lognormal pdf was supported in the laboratory measurements conducted. The findings were consistent with the field measurements, were no deviations from the lognormal pdf were detected. Minor deviations from this distribution were caused by images corrupted from reflections. The results for the parameters  $\sigma$  and  $m$  of the logarithmic normal distribution can be seen in Table 5.

[72] The net heat flux was estimated from the techniques presented in sections 7.1 and 7.2. The results for the heat flux at this high temporal resolution are presented in Figure 15. Here  $j_{\text{root}}$  for one image sequence is presented as well as for a whole deployment. Results for four deployments are presented in Table 6.

[73] The main difference between the estimate based on  $j_{\text{root}}$  or  $j_{\text{pdf}}$  can thus be stated as the higher resolution of  $j_{\text{root}}$  as it is not statistically based. Also, since fewer assumptions are needed for its derivation, this method is clearly favored. Nevertheless it is interesting to compare the performance of both techniques under a variety of conditions. This represents another verification of the assumptions made in estimating  $j_{\text{pdf}}$ . If both techniques estimate the same value for the net heat flux it can be inferred indirectly that the probability density function  $p(\tau)$  accurately models the statistical properties of the surface renewal process.

[74] Meteorological measurements of heat fluxes from the eddy correlation technique were conducted on board the R/V *Ronald H. Brown* (J. E. Hare, personal communication, 2001). Apart from verifying consistent results of both estimates  $j_{\text{root}}$  and  $j_{\text{pdf}}$  to one another, the results were also compared to the estimates based on those meteorological techniques  $j_{\text{met}}$ . A typical deployment is shown in Figure 15.

It can generally be stated that there exists a good agreement between the estimates. Within the margin of error, the agreement with the meteorologically derived heat flux estimates  $j_{\text{met}}$  seems to be quite good. Also there seems to be a slight correlation to the wind speed, as can be seen in Figure 15a, where peaks in the heat flux are followed by peaks in the wind velocity. However, it should be noted that measurements of the meteorological data were conducted on the bow tower of the research vessel, whereas the techniques based on thermography were conducted on LADAS. Both were separated by about 100 m during the measurements.

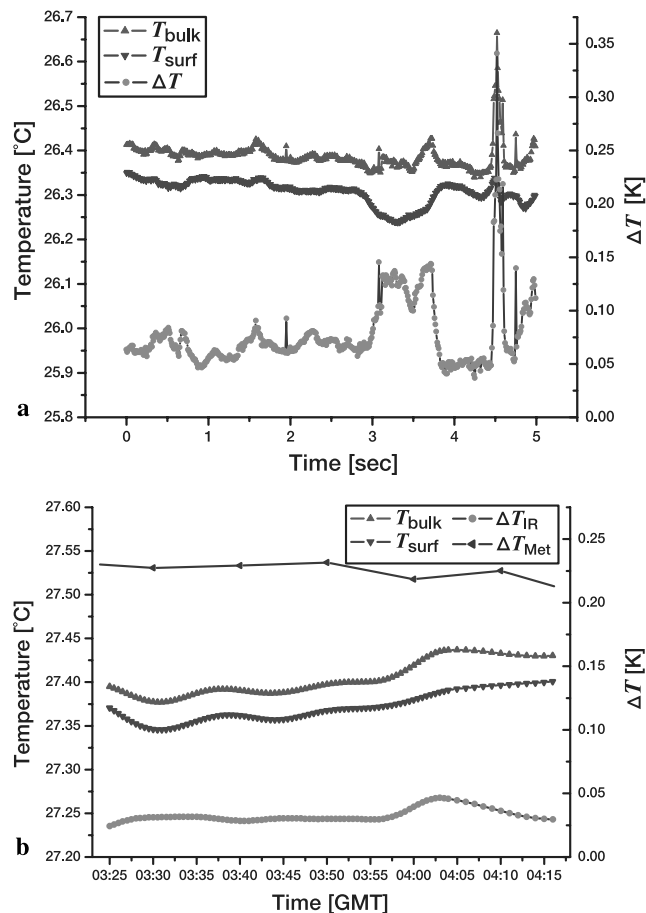


**Figure 13.** The temperature of both the bulk  $T_{\text{bulk}}$  and surface  $T_{\text{surf}}$  as well as the temperature difference  $\Delta T$  for typical deployment. (a) The estimated values for one sequence is shown (year day 58, 2001). (b) The whole data set for the whole deployment of year day 54, 2001, is shown where the values are compared to the ones derived from micrometeorological measurements. See color version of this figure in the HTML.

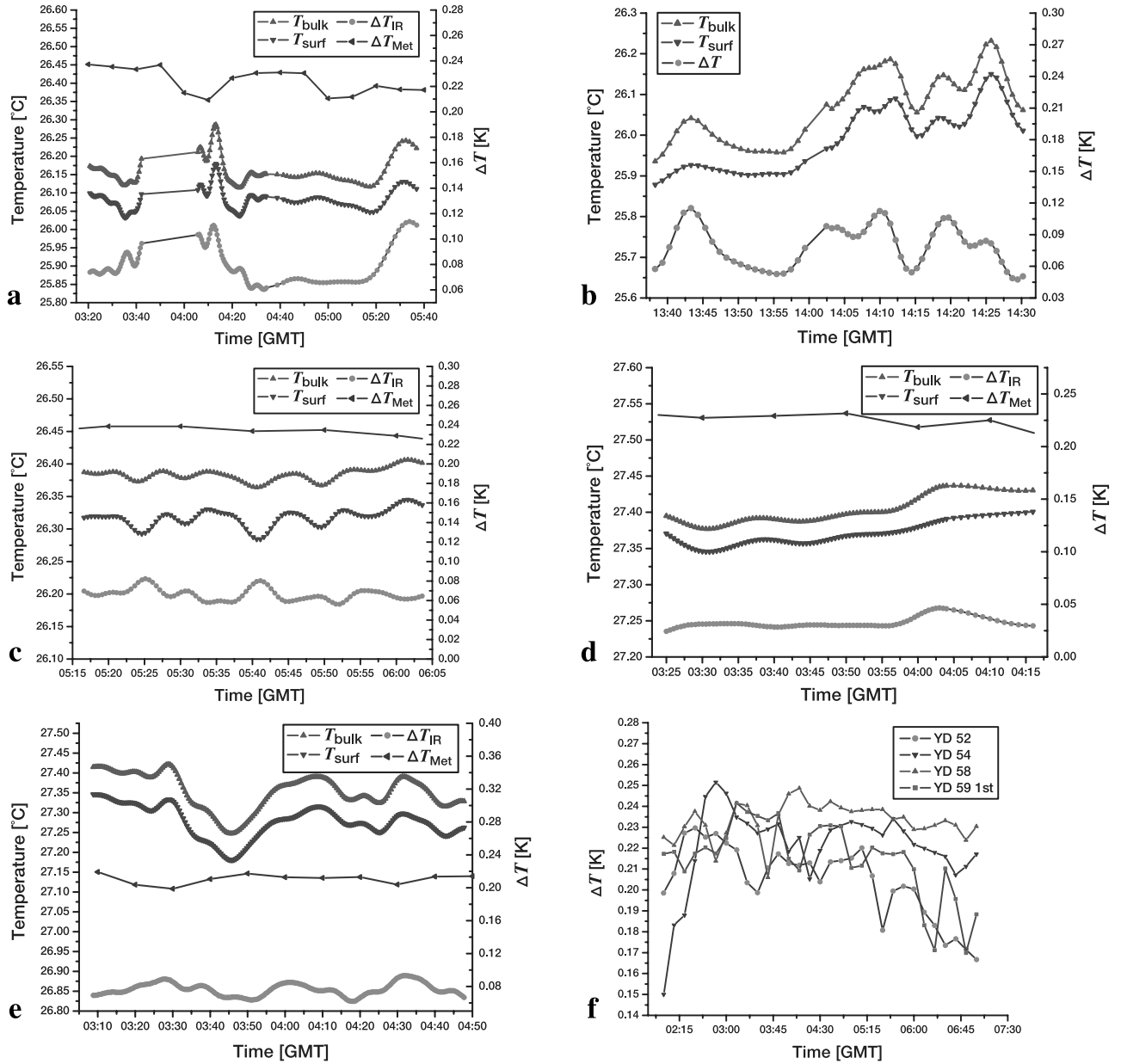


**Figure 14.** The temperature of both the bulk  $T_{\text{bulk}}$  and surface  $T_{\text{surf}}$  as well as the temperature depression  $\Delta T$ . From the deployments on (a)–(b) year day 59 and from the deployments on year day (c) 58, (d) 54, and (e) 52, as well as the equivalent data obtained from (f) J. E. Hare (personal communication, 2001) for the corresponding deployments. See color version of this figure in the HTML.

[75] From the measurements of the net heat flux the transfer velocities of heat can be computed according to equation (1). In order to compare these results to those of different trace gases these transfer velocities of heat can be scaled to that of  $\text{CO}_2$  at a temperature of  $20^\circ\text{C}$  ( $k_{600}$ ). Here use is made of equation (2). The results of these heat transfer measurements are presented in Table 7.

## 12. Conclusions

[76] The application of a surface renewal model to infrared imagery was presented. An important quantity of the proposed surface renewal model is the probability of surface renewals taking place. This probability is expressed

by the probability density function of times in between consecutive surface renewal events  $p(\tau)$ . Assuming this pdf to be lognormally distributed, we derived an analytical function for the frequency data of the surface temperature at the sea surface  $T_{\text{surf}}$ . Parameters of this analytical function are the bulk temperature  $T_{\text{bulk}}$  and the net heat flux  $j$ , apart from the parameters describing the lognormal distribution. The excellent agreement of this analytical function fitted to the frequency data of  $T_{\text{surf}}$  can be seen as an indirect verification of the assumption made in deriving this function. This assumption is the surface renewal model with the probability of surface renewal events to be distributed lognormally. Apart from verifying this assumption through the fit, the bulk temperature  $T_{\text{bulk}}$  can be gained from the

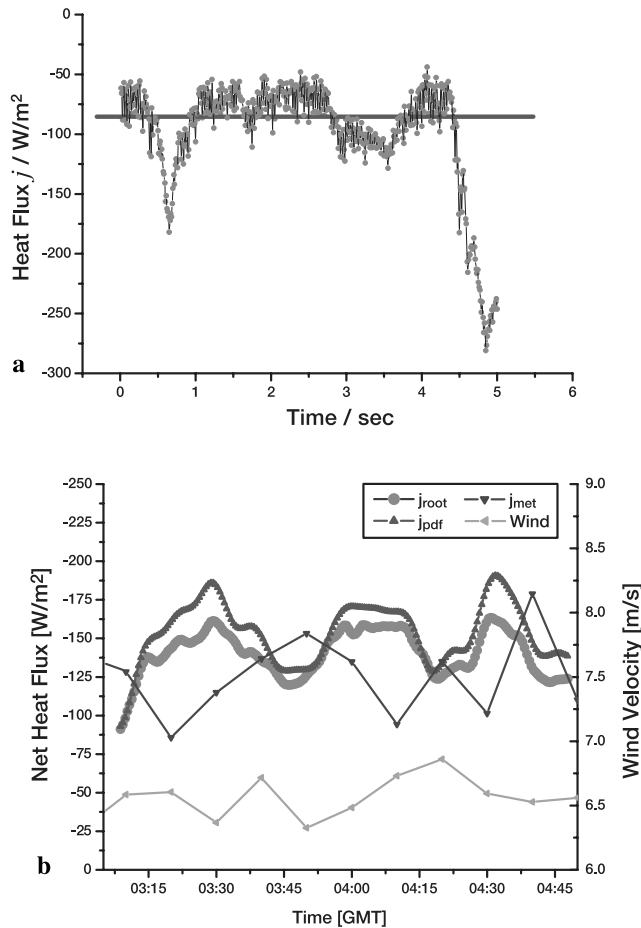


**Figure 15.** (a) The estimated net heat flux for one sequence of year day 58, 2001. (b) The flux estimate for the whole deployment of year day 52, 2001. Plotted are the estimates of  $j_{\text{root}}$ ,  $j_{\text{pdf}}$  and the one derived from meteorological techniques,  $j_{\text{met}}$ , as well as the wind velocity. See color version of this figure in the HTML.

distribution of the sea surface temperatures. We examine this technique on synthetic data and perform an error analysis of estimating  $T_{\text{bulk}}$  under varying noise levels of the input data. For the noise levels of current IR cameras the accuracy of retrieving the bulk temperature is found to be 3 mK. Schimpf *et al.* [2004] verified these findings in laboratory measurements.

[77] From modern digital image sequence analysis, the total derivative of the sea surface temperature with respect to time can be estimated. From this total derivative the time of residence of a water parcel at the sea surface  $\tau$  is computed at every pixel of the infrared image sequence. Analyzing the frequency data of  $\tau$  gives a direct verification of the pdf. We show that a lognormal distribution describes this frequency data very well. From a fit of the lognormal distribution to the frequency data, its parameters  $\sigma$  and  $m$  can be gained. Assuming the proposed surface renewal model with the lognormal pdf, an expression of the net heat flux  $j_{\text{pdf}}$  is derived. With this formulation  $j_{\text{pdf}}$  can be computed from the parameters  $\sigma$  and  $m$ . This net heat flux  $j$  is compared to the accurately known net heat flux under

laboratory conditions. The excellent agreement of the measured flux poses another indirect verification of the surface renewal model together with its lognormally distributed pdf. Making no assumption concerning the pdf of surface renewal, another expression for the net heat flux  $j_{\text{root}}$  is derived on the basis of the model of surface renewal alone. From this expression the net heat flux can be estimated from thermal infrared image sequences at the frame rate of the IR imager at pixel resolution. This allows for accurate, both temporally and spatially highly resolved heat flux measurements. Results of measurements with an spatial resolution of  $1.5 \times 1.5 \text{ mm}^2$  and a temporal resolution of 10 ms at a relative error of 5% are presented. Measurements both under laboratory and field conditions are shown. Results of the transfer velocity are compared to those of  $\text{N}_2\text{O}$  under laboratory conditions. A discrepancy of 30% was detected, the reason for which has to be addressed in future experiments.

[78] All of this demonstrates that the presented surface renewal model with a lognormal pdf is a good approximation of the transport of heat through the sea surface interface. The model produces consistent results for the estimation of different parameters of ocean-atmosphere heat transfer. The results are also applicable for the transfer of gas. This is due to Schmidt number scaling, from which the transfer velocity of mass can be deduced from the transfer velocity of heat. The presented model together with its application to infrared thermography is an interesting tool for analyzing the effect of waves, bubbles, rain and surfactants on the transfer of heat and mass.

## Appendix A: Temperature Distribution at the Sea Surface

[79] The underlying equation is that of thermal conduction at the interface

$$\Delta T(t) = T(t) = \frac{2j}{\sqrt{\pi\kappa c_p \rho}} \sqrt{\Delta t} = \alpha j \sqrt{\Delta t}, \quad t \geq t_0 \quad (\text{A1})$$

with  $\Delta t = t - t_0$  and  $\alpha = 2/(\sqrt{\pi\kappa c_p \rho})$ , which leads to the following expression for  $\Delta t$ :

$$\Delta t(T) = \frac{\pi\kappa c_p^2 \rho^2}{4j^2} T^2 = \left(\frac{T}{\alpha j}\right)^2. \quad (\text{A2})$$

We are interested in the probability of measuring a certain temperature  $T$ . This likelihood is higher when the change of temperature with respect to time is smaller. The gradient  $\partial/\partial T \Delta t(T)$  represents a mean to express the time it takes for the temperature to change over an infinitesimal interval  $\partial T$ . This is directly proportional to the probability of measuring the temperature  $T$ . The probability  $p(T|\tau)$  of measuring a

**Table 6.** Results of the GasExII Net Heat Flux Measurements<sup>a</sup>

Year Day	Wind Speed, m/s	$u_*$	$j_{\text{met}}$ , W/m <sup>2</sup>	$j_{\text{root}}$ , W/m <sup>2</sup>	$j_{\text{pdf}}$ , W/m <sup>2</sup>
52	5.23	0.199	-129.06	-141 ± 7	-145 ± 7
54	4.18	0.154	-116.60	-124 ± 6	-91 ± 5
58	5.05	0.184	-142.47	-143 ± 7	-154 ± 8
59	4.76	0.170	-119.65	-121 ± 6	-113 ± 6

<sup>a</sup>The errors of the meteorological estimates are not known.

**Table 7.** Transfer Velocities of Heat, Scaled to a Schmidt Number of  $Sc = 600^a$ 

Year Day	Wind Speed, m/s	$u_*$ , m/s	$k_{600,roots}$ , cm/h	$k_{600,pdf}$ , cm/h
52	5.23	0.199	18.08 ± 0.92	18.56 ± 0.95
54	4.18	0.154	38.28 ± 1.95	28.33 ± 1.45
58	5.05	0.184	20.18 ± 1.03	21.63 ± 1.10
59	4.76	0.170	14.03 ± 0.72	13.08 ± 0.67

<sup>a</sup>Because of the interface conditions the Schmidt number exponent  $n = 1/2$  was used.

temperature  $T$  at a given time  $\tau$  between surface renewals is thus given by

$$p(T|\tau) = \begin{cases} \gamma \frac{\partial t(T)}{\partial T} = \gamma \frac{2T}{(\alpha j)^2}, & \forall 0 \leq t \leq \tau \\ 0 & \forall t > \tau \end{cases}, \quad (A3)$$

with a constant of proportionality  $\gamma$ . This constant can be solved by normalizing  $p(T|\tau)$  and using equation (A1):

$$1 \equiv \int_0^{\tau(\tau)} p(T|\tau) dT = \frac{\gamma T^2}{(\alpha j)^2} \Big|_0^{\tau(\tau)} = \gamma \cdot \tau. \quad (A4)$$

Thus  $\gamma = \frac{1}{\tau}$ .

[80] The likelihood  $p(T)$  of measuring the temperature  $T$  can then be calculated if the probability  $p(\tau)$  of the time  $\tau$  between surface renewals is known, that is

$$p(T) = \int_0^{\infty} p(T|\tau) \cdot p(\tau) d\tau = \frac{2T}{(\alpha j)^2} \int_0^{\infty} \frac{p(\tau)}{\tau} d\tau. \quad (A5)$$

[81] The probability density function  $p(\tau)$  is a priori unknown. In section 2 experimental evidence was presented that a lognormal distribution as given by equation (5) is very likely. Therefore inserting equation (5) for  $p(\tau)$  into equation (A5) results in

$$p(T) = \frac{2T}{(\alpha j)^2 \sqrt{\pi} \sigma} \int_{t(T)}^{\infty} \frac{e^{-\frac{(\ln \tau - m)^2}{\sigma^2}}}{\tau^2} d\tau. \quad (A6)$$

[82] The integral in this equation can be solved by introducing the substitute  $x = \ln \tau$  which means that  $d\tau = \tau dx$ . Thus

$$\begin{aligned} \int_{t(T)}^{\infty} \frac{\exp\left[-\frac{(\ln \tau - m)^2}{\sigma^2}\right]}{\tau^2} d\tau &= \int_{\ln t(T)}^{\infty} \frac{\exp\left[-\frac{(x - m)^2}{\sigma^2}\right]}{\exp[x]} dx \\ &= \int_{\ln t(T)}^{\infty} \exp\left[-\frac{1}{\sigma^2} x^2 + \left(\frac{2m}{\sigma^2} - 1\right)x - \frac{m^2}{\sigma^2}\right] dx. \end{aligned} \quad (A7)$$

From integration tables [Beyer, 1984] this integral can be solved. The probability density function  $p(T)$  is thus given

from equation (A6) and making use of the expression (A2) for  $t(T)$ , which leads to

$$\begin{aligned} p(T_{\text{surf}}) &= \frac{T_{\text{surf}} - T_{\text{bulk}}}{(\alpha j)^2} \exp\left[\frac{\sigma^2}{4} - m\right] \operatorname{erfc} \\ &\quad \cdot \left[\frac{\sigma}{2} - \frac{m}{\sigma} + \frac{1}{\sigma} \ln\left(\frac{T_{\text{surf}} - T_{\text{bulk}}}{\alpha j}\right)^2\right], \quad (A8) \\ &\text{with } \alpha = \frac{2}{\sqrt{\pi \kappa \rho c_p}}. \end{aligned}$$

Here the complementary error function is defined as  $\operatorname{erfc}(z) = 1 - \operatorname{erf}(z)$  and the error function given by the integral of the Gaussian distribution  $\operatorname{erf}(z) = 2/\sqrt{\pi} \int_0^z \exp(-\eta^2) d\eta$ .

[83] **Acknowledgments.** The authors would like to thank the three anonymous reviewers who helped to improve the quality of this paper through their comments. Also, the authors would like to thank Wade R. McGillis and Jeff Hare for supplying meteorological estimates of the sea surface heat fluxes during the GasExII cruise. The authors acknowledge the assistance of the crew of the NOAA ship *Ronald H. Brown* during the GasExII study. For fruitful discussions on topics of this manuscript, the authors would like to thank Nelson M. Frew and Tetsu Hara. This work was supported in part by the German Science Foundation (DFG) through the research unit FOR240 ‘‘Image Sequence Processing to Investigate Dynamic Processes’’. Financial support to participate in the GasExII cruise was granted by NOAA (NOAA Grant NAO6GP0487) as was the data analysis of the measurements conducted during that cruise (NOAA Grant NA16GP2918).

## References

- Asher, W. E., and R. Wanninkhof (1993), The effect of bubble-mediated gas transfer on purposeful dual-gaseous tracer experiments, *J. Geophys. Res.*, *103*, 10,555–10,560.
- Beyer, W. H. (1984), *CRC Standard Mathematical Tables*, 27th ed., CRC Press, Boca Raton, Fla.
- Brutsaert, W. (1975a), A theory for local evaporation (or heat transfer) from rough to smooth surfaces at ground level, *Water Resource Res.*, *11*, 543–550.
- Brutsaert, W. (1975b), The roughness length for water vapor, sensible heat, and other scalars, *J. Atmos. Sci.*, *32*, 2028–2031.
- Danckwerts, P. V. (1951), Significance of a liquid-film coefficients in gas absorption, *Ind. Eng. Chem.*, *43*, 1460–1467.
- Fairall, C. W., E. F. Bradley, J. S. Godfrey, G. A. Wick, J. B. Edson, and G. S. Young (1996a), Cool-skin and warm-layer effects on sea surface temperature, *J. Geophys. Res.*, *101*, 1295–1308.
- Fairall, C. W., E. F. Bradley, D. P. Rogers, J. B. Edson, and G. S. Young (1996b), Bulk parameterization of air-sea fluxes for tropical ocean-global atmosphere coupled-ocean atmosphere response experiment, *J. Geophys. Res.*, *101*, 3747–3764.
- Fairall, C. W., et al. (2000), Parameterization and micrometeorological measurements of air-sea gas transfer, *Boundary Layer Meteorol.*, *96*, 63–105.
- Garbe, C. S., and B. Jähne (2001), Reliable estimates of the sea surface heat flux from image sequences, in *Pattern Recognition: Proceedings of the 23rd DAGM Symposium, Lecture Notes Comput. Sci.*, vol. 2191, edited by B. Radig and S. Florczyk, pp. 194–201, Springer-Verlag, New York.
- Garbe, C. S., H. Haußecker, and B. Jähne (2001), Measuring the sea surface heat flux and probability distribution of surface renewal events, in *Gas Transfer at Water Surfaces, Geophys. Monogr. Ser.*, vol. 127, pp. 109–114, edited by M. Donelan et al., AGU, Washington, D. C.
- Garbe, C. S., H. Spies, and B. Jähne (2002), Mixed ols-tls for the estimation of dynamic processes with a linear source term, in *Pattern Recognition: Proceedings of the 24th DAGM Symposium, Lecture Notes Comput. Sci.*, vol. 2449, edited by L. Van Gool, pp. 463–471, Springer-Verlag, New York.
- Garbe, C. S., H. Spies, and B. Jähne (2003), Estimation of surface flow and net heat flux from infrared image sequences, *J. Math. Imaging Vision*, *19*, 159–174.
- Geernaert, G. L. (1999), Theory of air-sea momentum, heat and gas fluxes, in *Air-Sea Exchange, Physics, Chemistry and Dynamics*, edited by G. L. Geernaert, pp. 25–48, Kluwer Acad., Norwell, Mass.

- Hariott, P. (1962), A random eddy modification of the penetration theory, *Chem. Eng. Sci.*, *17*, 149–154.
- Haußecker, H. (1996), Messung und Simulation von kleinskaligen Austauschvorgängen an der Ozeanoberfläche mittels Thermographie, Ph.D. thesis, Univ. of Heidelberg, Heidelberg, Germany.
- Haußecker, H., and D. J. Fleet (2001), Computing optical flow with physical models of brightness variation, *Pattern Anal. Mach. Intel.*, *23*, 661–673.
- Haußecker, H., et al. (1999), A total least squares for low-level analysis of dynamic scenes and processes, in *DAGM Symposium*, edited by W. Förstner et al., pp. 240–249, Springer-Verlag, New York.
- Haußecker, H., U. Schimpf, C. S. Garbe, and B. Jähne (2001), Physics from IR image sequences: Quantitative analysis of transport models and parameters of air-sea gas transfer, in *Gas Transfer at Water Surfaces*, *Geophys. Monogr. Ser.*, vol. 127, pp. 103–108, edited by M. Donelan et al., AGU, Washington, D. C.
- Higbie, R. (1935), The rate of absorption of a pure gas into a still liquid during short periods of exposure, *Trans. Am. Inst. Chem. Eng.*, *31*, 365–389.
- Jähne, B. (1980), Parametrisierung des Gasaustausches mit Hilfe von Laborexperimenten, Ph.D. thesis, Inst. für Umweltpophys., Univ. of Heidelberg, Heidelberg, Germany.
- Jähne, B., et al. (1989), Investigating the transfer process across the free aqueous boundary layer by the controlled flux method, *Tellus, Ser. B*, *41*, 177–195.
- Jähne, B., H. Haußecker, H. Scharr, H. Spies, D. Schmundt, and U. Schurr (1998), Study of dynamical processes with tensor-based spatiotemporal image processing techniques, in *Computer Vision—ECCV'98, Proceedings of the 5th European Conference on Computer Vision*, vol. II, *Lecture Notes in Comput. Sci., LNCS 1407*, pp. 322–336, Springer-Verlag, New York.
- Jessup, A. T., et al. (1997a), Infrared remote sensing of breaking waves, *Nature*, *385*, 52–55.
- Jessup, A. T., C. J. Zappa, and H. H. Yeh (1997b), Defining and quantifying microscale wave breaking with infrared imagery, *J. Geophys. Res.*, *102*, 23,145–23,153.
- Kolmogorov, A. N. (1962), A refinement of previous hypotheses concerning the local structure of turbulence in a viscous incompressible fluid at high Reynolds number, *J. Fluid Mech.*, *13*, 82–85.
- Kraus, E. B., and J. A. Businger (1994), *Atmosphere-Ocean Interaction*, *Oxford Monogr. Geol. Geophys.*, vol. 27, 2nd ed., Oxford Univ. Press, New York.
- Leibovich, S. (1983), The form and dynamics of Langmuir circulations, *Annu. Rev. Fluid Mech.*, *15*, 391–427.
- Liu, W. T., and J. A. Businger (1975), Temperature profile in the molecular sublayer near the interface of a fluid in turbulent motion, *Geophys. Res. Lett.*, *2*, 4031975.
- Liu, W. T., K. B. Katsaros, and J. A. Businger (1979), Bulk parameterization of air-sea exchanges of heat and water vapor including the molecular constraints at the interface, *J. Atmos. Sci.*, *36*, 1722–1735.
- McGillis, W. R., J. B. Edson, J. E. Hare, and C. W. Fairall (2001), Direct covariance air-sea CO<sub>2</sub> fluxes, *J. Geophys. Res.*, *106*, 16,729–16,745.
- McWilliams, J. C., P. P. Sullivan, and C.-H. Moeng (1997), Langmuir turbulence in the ocean, *J. Fluid Mech.*, *334*, 1–30.
- Melville, W. K., R. Shear, and F. Veron (1998), Laboratory measurements of the generation and evolution of Langmuir circulations, *J. Fluid Mech.*, *364*, 31–58.
- Negahdaripour, S., and C. H. Yu (1993), A generalized brightness change model for computing optical flow, paper presented at International Conference in Computer Vision, Inst. of Electr. and Electr. Eng., Berlin.
- Plueddemann, A. J., J. A. Smith, D. M. Farmer, R. A. Weller, W. R. Crawford, R. Pinkel, S. Vagle, and A. Gnanadesikan (1996), Structure and variability of Langmuir circulation during the surface waves processes program, *J. Geophys. Res.*, *101*, 3525–3543.
- Prema (2000), *User Manual Prema 3040 High Precision Thermometer*, Mainz, Germany.
- Rao, K. N., R. Narasimah, and M. B. Narayanan (1971), The “bursting” phenomenon in a turbulent boundary layer, *J. Fluid Mech.*, *48*, 339–352.
- Schimpf, U. (2000), Untersuchung des Gasaustausches und der Mikroturbulenz an der Meeresoberfläche mittels Thermographie, Ph.D. thesis, Univ. of Heidelberg, Heidelberg, Germany.
- Schimpf, U., C. Garbe, and B. Jähne (2004), Investigation of transport processes across the sea-surface microlayer by infrared imagery, *J. Geophys. Res.*, *109*, C08S13, doi:10.1029/2003JC001803.
- Soloviev, A. V., and P. Schlüssel (1994), Parameterization of the cool skin of the ocean and the air-ocean gas transfer on the basis of modeling surface renewal, *J. Phys. Oceanogr.*, *24*, 1339–1346.
- Soloviev, A. V., and P. Schlüssel (1996), Evolution of cool skin and direct air-sea gas transfer coefficient during daytime, *Boundary Layer Meteorol.*, *77*, 45–68.
- Taylor, G. (1938), The spectrum of turbulence, *Proc. R. Soc., London*, *102*, 817–822.
- Van Huffel, S., and J. Vandewalle (1991), *The Total Least Squares Problem: Computational Aspects and Analysis*, Soc. for Ind. and Appl. Math., Philadelphia, Pa.
- Veron, F., and W. K. Melville (2001), Experiments on the stability and transition of wind-driven water surfaces, *J. Fluid Mech.*, *446*, 25–65.
- Ward, B., and S. Redfern (1999), A neural network model for predicting the bulk-skin temperature difference at the sea surface, *Int. J. Remote Sens.*, *20*, 3533–3548.
- Wick, G. A., et al. (1996), The behavior of the bulk-skin sea surface temperature difference under varying wind speed and heat flux, *J. Phys. Oceanogr.*, *26*, 1969–1988.
- Zhang, D., and M. Herbert (1999), Harmonic maps and their applications in surface matching, paper presented at 1999 Conference on Computer Vision and Pattern Recognition, Inst. of Electr. and Electr. Eng., Fort Collins, Colo.

C. S. Garbe and B. Jähne, Interdisciplinary Center for Scientific Computing, University of Heidelberg, Im Neuenheimer Feld 368, D-69120 Heidelberg, Germany. (christoph.garbe@iwr.uni-heidelberg.de; bernd.jaehne@iwr.uni-heidelberg.de)

U. Schimpf, Institute of Environmental Physics, University of Heidelberg, Im Neuenheimer Feld 229, D-69120 Heidelberg, Germany. (uwe.schimpf@iwr.uni-heidelberg.de)